



# The AETHER project: development of air-breathing electric propulsion for VLEO missions

T. Andreussi<sup>1</sup> · E. Ferrato<sup>1</sup> · C. A. Paissoni<sup>1</sup> · A. Kitaeva<sup>1</sup> · V. Giannetti<sup>1</sup> · A. Piragino<sup>1</sup> · S. Schäff<sup>2</sup> · K. Katsonis<sup>3</sup> · Ch. Berenguer<sup>3</sup> · Z. Kovacova<sup>4</sup> · E. Neubauer<sup>4</sup> · M. Tisaev<sup>5</sup> · B. Karadag<sup>5</sup> · A. Lucca Fabris<sup>5</sup> · M. Smirnova<sup>6</sup> · A. Mingo<sup>6</sup> · D. Le Quang<sup>7</sup> · Z. Alsalihi<sup>7</sup> · F. Bariselli<sup>7</sup> · P. Parodi<sup>7</sup> · P. Jorge<sup>7</sup> · T. E. Magin<sup>7</sup>

Received: 31 August 2021 / Revised: 24 March 2022 / Accepted: 25 March 2022 / Published online: 29 April 2022  
© The Author(s), under exclusive licence to Council of European Aerospace Societies 2022

## Abstract

The possibility of efficiently exploiting Very Low Earth orbits (VLEO) poses significant technological challenges. One of the most demanding constraints is the need to counteract the drag generated by the interaction of the spacecraft with the surrounding atmosphere. Funded by the European Commission under the H2020 programme, the Air-breathing Electric Thruster (AETHER) project aims at developing the first propulsion system able to maintain a spacecraft at very-low altitudes for an extended time. The main objective of the project is to demonstrate, in a relevant environment, the critical functions of an air-breathing electric propulsion system, and its effectiveness in compensating atmospheric drag. This achievement will involve multiple research activities, among which: (i) the characterization of specific application cases through an extensive market analysis in order to define specific requirements and constraints at different design levels, (ii) fulfilment of pertinent testing conditions of flight conditions on-ground, relevant to the specific mission cases, (iii) the development of critical technologies, in particular those relevant to the collection, the ionization and the acceleration of rarefied atmospheric mixtures and (iv) the testing of the RAM-EP thruster to assess the system performance. In this paper, the main activities foreseen in the AETHER project are described, providing the detailed perspective towards an effective exploitation of the project outcomes for a possible future in-orbit demonstration.

**Keywords** Air-breathing electric propulsion · Plasma thruster · Very low Earth orbit · Rarefied air flow

---

✉ T. Andreussi  
tommaso.andreussi@sitael.com

S. Schäff  
sven.schaeff@astros.de

K. Katsonis  
katsonis.dedalos@gmail.com

E. Neubauer  
e.ne@rhp.at

A. Lucca Fabris  
a.luccafabris@surrey.ac.uk

M. Smirnova  
maria.smirnova@transmit.de

D. Le Quang  
lequang@vki.ac.be

<sup>1</sup> SITAE S.P.A., Via A. Gherardesca 5, 56121 Pisa, Italy

<sup>2</sup> Astos Solutions GmbH, Meitnerstr. 8, 70563 Stuttgart, Germany

<sup>3</sup> DEDALOS Ltd., Vas. Olgas 128, 54645 Thessaloniki, Greece

<sup>4</sup> RHP-Technology GmbH, 2444 Seibersdorf, Austria

<sup>5</sup> Surrey Space Centre, University of Surrey, Guildford GU2 7XH, UK

<sup>6</sup> TransMIT Gesellschaft Für Technologietransfer mbH, 35394 Giessen, Germany

<sup>7</sup> Von Karman Institute for Fluid Dynamics, 1640 Sint-Genesius-Rode, Belgium

## 1 Introduction

The exploitation of Very Low Earth Orbits (VLEOs) would provide a new set of potentially market-disruptive mission opportunities, see [1]. Low-altitude orbits would enable a further improvement of the resolution for observation missions, low latency and high revisit time for telecommunication missions, as well as new scientific opportunities for the investigation of both the upper layers of the atmosphere and Earth's gravitational field. Despite the significant advantages, the main criticalities for spacecraft operating at such low altitude is the drag generated by the upper layers of the atmosphere. Below 250 km, the drag needs to be effectively compensated to avoid a rapid decay of the orbit.

Air-breathing electric propulsion, often shortened as ABEP or ram-EP, is emerging as a viable concept offering a disruptive approach to overcome the challenge posed by VLEO missions [2–16]. A ram-EP system is composed of an intake and an electric thruster. The intake is used to collect the atmospheric gas molecules and direct them to the thruster/accelerator, possibly increasing the pressure in a compression stage. The collected particles are then ionized by the thruster, accelerated, and expelled at high exhaust velocity to generate thrust. A power system, likely a combination of solar arrays and batteries, provides the required electric power. As a result, the adoption of ram-EP devices would provide thrust generation in VLEO without any on-board propellant. This would allow to mitigate the limitations on the spacecraft lifetime imposed by the drag, reducing, at the same time, the spacecraft total wet mass.

The air-breathing EP technology comes with several criticalities, mainly associated to system performance, lifetime, and integration into platform. First, VLEO atmosphere is characterized by a highly variable composition depending on solar activity and orbital parameters, being  $N_2$  and O the major constituents (> 95%). Due to the chemical aggressiveness of atomic oxygen (ATOX), material degradation is a major concern. Electrodes directly exposed to the atmospheric plasma discharge may be quickly oxidized and become electrically insulating, leading to a premature thruster failure. This is particularly true for hollow cathodes and neutralizers, which are commonly used in both conventional Ion and Hall thrusters. Therefore, a non-competitive lifetime is the main technology risk. Moreover, the high variability characterizing VLEO atmosphere poses a great challenge on platform power and thrust management capability, as variations of inlet flow density and, thus, discharge power consumption (at least, for a constant operating voltage) of more than  $\pm 50\%$  can be expected. The development of any air-breathing

technology should thus cope with the need of devising innovative power management and thrust strategies to safely operate all the platform subsystems and maintain the targeted mission profile.

In the framework of the Horizon-2020 AETHER programme, funded by the European Commission, a novel air-breathing propulsion system is being developed to operate in VLEO environment. In the present paper, we provide the rationale followed for platform and propulsion requirement derivation, describing the main ram-EP system components design, performance, and criticalities together with a review of the main activities performed during the AETHER project. It is important to highlight that, due to the complexity and the relative low maturity of the air-breathing technology, we decided to follow a technology-push approach, identifying the optimal conditions for the operation of the propulsion system without strict constraints related to specific mission scenarios or payloads. As a matter of fact, the main objective of the AETHER programme is to characterize the operation of an air-breathing thruster prototype. In case of a successful demonstration, AETHER's output would allow to have the necessary dataset which, in the framework of further development activities and realization of more advanced air-breathing thruster models, would allow to iterate on and refine both propulsion system and platform design with more focus on user requirements and stakeholders needs.

In Sect. 2, after a description of the selected mission profile and the characterization of the residual atmosphere at the altitudes of interest, we present an overview of the air-breathing propulsion subsystem, highlighting the requirements that need to be satisfied for an effective drag compensation. Then, results of mission analysis are presented. The orbit propagation considers the drag resulting from the presence of atmospheric particles and the thrust generated by the air-breathing thruster with the power available on-board. In Sect. 3, we describe the optimization of the platform design, and of the intake that collects the residual atmospheric particles and performs the passive compression of the incoming flow. Then, the core stages of the air-breathing thruster are presented in Sect. 4, in which the main technical solutions adopted to ionize and accelerate the gathered particles are described together with a simple model of the expected propulsive performance. Section 5 is then dedicated to the development of a cathode/neutralizer technology able to operate with atmospheric propellant, which represents a main challenge of the programme. In Sect. 6, we report the on-going activities dedicated to on-ground testing, focusing on the experimental characterization of a particle flow generator, as well as on the development of advanced invasive and non-invasive diagnostics. The test activities, which are used also to investigate the interaction between the energetic atmospheric flow and the propulsion subsystem materials, are also described. Finally, in Sect. 7, we summarize

the main results obtained by the AETHER consortium in the first part of the programme and the perspectives for the development of VLEO missions.

## 2 Mission analysis and requirement derivation

### 2.1 Mission scenario: challenges and definition

A reference mission scenario has been introduced to investigate the operation of the thruster as well as to provide main mission and platform characteristics. The considered mission scenario foresees the VLEO spacecraft operated in an In-Orbit demonstration (IOD) mission, with the specific goal of demonstrating the operability of the thruster for an extended mission lifetime and its robustness to the different atmospheric seasonal variations. The preliminary high-level requirements derived for the air-breathing platform hosting the proposed air-breathing propulsion system are provided in Table 1. The proposed concept is a medium class platform. Considering that efficient thruster operation is required to compensate drag and that EP thruster efficiency tends to improve significantly with size, such a platform size was chosen as a good compromise between platform class (the main driver was its envelope compatibility with VEGA-C launcher) and expected vs required thruster efficiency. At current stage, about 1.5 m<sup>3</sup> of volume are available behind the intake wake for low-drag integration of the payload and other platform subsystems, while the power system is based on about 11 m<sup>2</sup> triple-junction GaAs body-mounted solar arrays and a 4.4 kWh battery pack. Due to the harsh environment characterizing VLEO, a main criticality is the possible occurrence of arcing phenomena between solar cells and platform structure or inside the intake. Such a risk shall clearly be investigated and mitigated from the very beginning of ram-EP platform design consolidation. Another main criticality is the loss of volume available for payload and other subsystems due to the internal intake, together

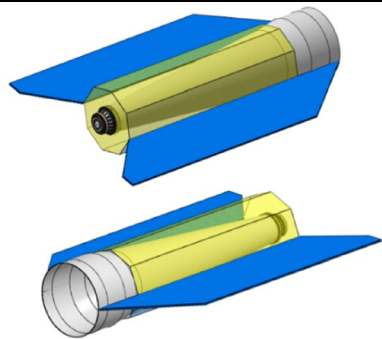
with intrinsic difficulties in ensuring an optimum center-of-gravity (CoG) position. In this regard, main platform electronics may be allocated as flat boards in the dark side of the solar arrays and as close as possible to the intake inlet, which would allow to move forward the CoG. The preliminary platform AOCS design is based on four magnetorquers, four micro-control gyros, four fine sun sensors, six coarse sun-earth sensors, three-star trackers and an inertial measurement unit. As a reference, at drag levels below 50 mN the GOCE S/C could guarantee 6 deg yaw/pitch by using magnetorquers only [17]. Note however that the permanent magnet included in the alternative neutralizer (see Sect. 5) together with the electromagnets included in the ram-EP thruster (see Sect. 4) may induce additional disturbance torques due to interaction with Earth's magnetic field. In this regard, requirement for attitude control may be more severe as compared to the GOCE mission.

Due the numerous criticalities of such an innovative platform and propulsion concept, the possibility to include a Xe tank on-board shall be properly evaluated as a backup solution. Even if the addition of tanks and valves poses the risk to reduce the attractiveness of the air-breathing EP concept, it may also lead to significant benefits:

- The cathode(s) can be fed by piping with the on-board Xe propellant, eliminating the risk related to cathode operation with oxygen. Note that the mass flow rate required by cathode operation is usually one order of magnitude lower than the one required by the thruster. As such, it is expected that the wet mass of a traditional EP system would still be significantly higher than the one of an air-breathing system featuring a pipe-fed cathode;
- In case of difficulties or anomalies in thruster ignition with atmospheric propellant in air-breathing mode, Xe propellant may be injected by an auxiliary ion stage injector so to facilitate ignition transients;
- Alternatively, the implementation of a tank on-board would allow to integrate a complete Xe EP system together with the airbreathing one. This design alterna-

**Table 1** High-level specifications of AETHER ram-EP platform

High-Level Platform Specifications	
Platform Mass	500 – 750 kg
Platform Power	2 – 3 kW
Operating Orbit	SS0 6am dawn dusk, 190 to 240 km
Platform Envelope	Compatible with Vega-C launcher
Available low-drag volume (behind intake wake)	1 – 1.5 m <sup>3</sup>



tive would allow to operate with Xe at higher altitudes (when the atmosphere is too rarefied to achieve air-breathing thruster ignition and operation) thus extending the platform capability range. Moreover, Xe propellant may be used for contingency in case the platform reaches a lower altitude with respect to the air-breathing system lower operation limit. In this case, the system may be operated with Xe until an altitude appropriate to air-breathing operation is again reached.

In any case, in the present work, we consider a single, fully-air-breathing system as the baseline. During the mission definition process, the preliminary assumption introduced is the possibility to continuously operate the thruster. According to this mission constraint, which has an impact on the onboard power management along the trajectory, the sun-synchronous orbit (SSO) dawn-dusk has been selected as reference orbit. In fact, the SSO is an optimal kind of orbit for several applications. Because illumination conditions are the same over a target area at the same time each day, it is perfectly suited for any kind of mapping and observation, no matter if scientific or commercial. Such applications include environmental monitoring and Earth observation (e.g., optical or radar) but also the remote study of the atmosphere. Moreover, a dawn-dusk SSO has shorter eclipse periods than differently inclined orbits and sun-synchronous orbits with other local time of the ascending node.

As introduced in Sect. 1, a major challenge of air-breathing electric propulsion is related with the strong coupling between the residual atmospheric properties, the propulsion system performance, the spacecraft architecture, and the mission itself. The high variability of the atmospheric properties with altitude, as well as with solar activity, implies a

variability of drag and thrust, which must be considered for a reliable mission analysis.

After the definition of a Design Reference Mission (DRM), we performed an assessment of atmospheric flow properties at different altitudes, characterizing the composition, temperature, density, and variability with respect to the solar activity of the residual atmosphere. Together with the modelling of ram-EP thruster performance (see Sect. 4), the assessment of atmospheric properties allowed for defining the necessary inputs for mission analysis.

## 2.2 Design reference mission

The DRM illustrated in Fig. 1 reports three possible mission profile alternatives derived considering: (i) the thrust over drag ratio, which is strictly related to the target altitudes, the number of phases where the average altitude is controlled around the selected target altitude and the duration of these phases; (ii) the operation during different solar periods (high, medium and low solar periods) with respect to the possible launch date which determines the S/C capability to control the average altitude around the target altitude and (iii) the launch capability of small-medium launchers.

The baseline profile consists of eight main phases (1 to 8). Phase 1 considers the launch of the spacecraft on an SSO dawn-dusk on the so-called “High operative altitude orbit”. After the separation from the upper stage of the launcher (Phase 2), the spacecraft enters in the commissioning phase where both subsystems’ status and operation are checked (Phase 3). This phase is followed by a descend phase where the altitude is decreased from High Operative Altitude to Medium Operative Altitude without operating the ram-EP thruster (Phase 4). In general, the injection altitude shall be carefully evaluated based on the designed commissioning

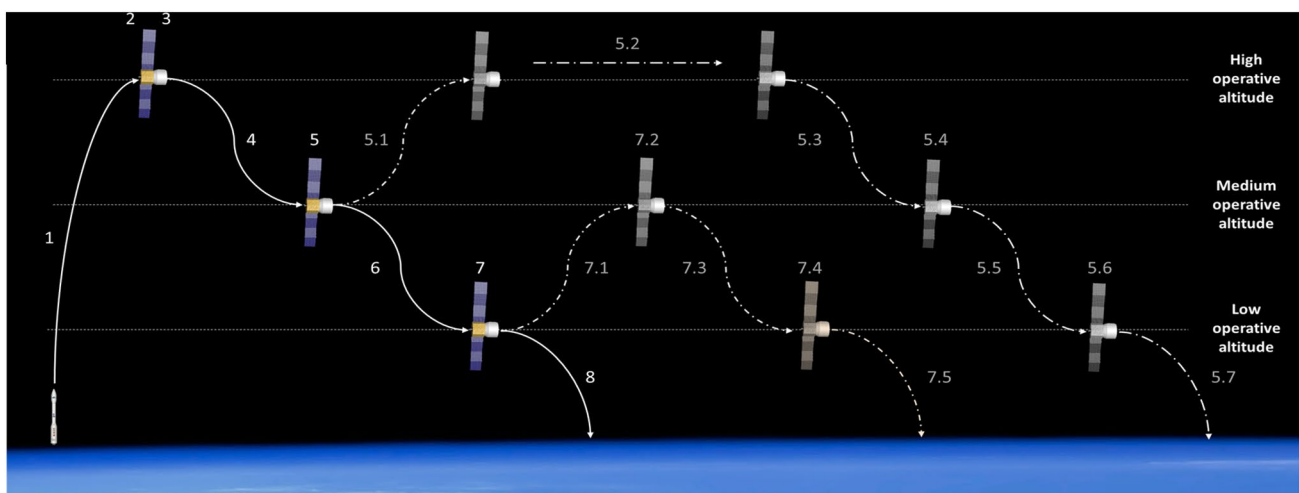


Fig. 1 Ram-EP IOD Design Reference Mission (DRM)

time: it shall be sufficiently high to ensure, with high margin, that commissioning duration (during which the spacecraft is unpropelled) will be significantly lower than the orbital decay time from the injection altitude to the propulsion system operative altitude range.

In the next phase, the spacecraft maintains a constant altitude of Medium Operative Altitude by operating the thruster in ON/OFF control cycles (Phase 5). After that, a second descend phase is planned to reach the minimum operative altitude at Low Operative Altitude (Phase 6). At this altitude, the ram-EP thruster is still able to provide a thrust over drag ratio greater than one (Phase 7). Phase 8 foresees the re-entry phase of the spacecraft. To fully prove the capability of the ram-EP spacecraft from phase 5 and phase 7 additional mission extension can be included. These extensions consist in a sequence of altitude raising and descending leg that could be opportunely introduced considering periodic atmospheric variations. Moreover, these phases can be cyclically repeated according to the imposed mission requirement to fully guarantee the demonstration of the ram-EP concept.

Even if a more detailed ConOps still must be assessed, especially based on the experimental verification of the ram-EP sub-system performance, we assume both payload and propulsion system to be always in ON status during illumination and in OFF status during eclipses. During eclipse, a battery pack provides power to the other active platform elements. With respect to PPU design applicable to standard EP devices, a main feature distinguishing the ram-PPU is the discharge control logic implementation, as it shall ensure an almost constant propulsion system power consumption also for highly variable inlet flow properties. Indeed, inlet flow density variation in the order of  $\pm 50\%$  can be expected throughout a single orbit in VLEO. The proposed discharge controller regulates the voltage applied to the thruster electrodes based on the discharge current and voltage. Such a control would allow to ensure a proper power management at system level, as a settable, constant power level is allocated to the propulsion system when in ON condition. This would also allow to temporarily reduce the ram-EP power consumption (by acting on the ram-EP power set point) in case a simultaneous power peaking of all the other subsystems exceeds the power available from solar arrays. On the other hand, in case more thrust is required during a particular mission phase, the payload may be temporarily switched OFF to increase the ram-EP power consumption set-point.

### 2.3 Assessment of atmospheric flow properties

Evaluation of the composition of the Earth atmosphere in various altitudes within the thermosphere and higher than the Karman line limit has been addressed at the very beginning of the project. Moreover, to widen the application cases of atmosphere-breathing propulsion, characteristics

of inner and of outer planets atmospheres and of natural satellites have been addressed. Towards this aim, the existing DEDALOS proprietary 4 Components Detailed Global Model (4CDGM) code has been used [18], together with an analogous Detailed Global Model (DGM) applicable to the case of Venus and Mars [19–21].

Specifically for the selected Earth case, the 4CDGM is a DGM for a gas composed by mixtures of nitrogen and of oxygen elements with initially given components of N, N<sub>2</sub>, O and O<sub>2</sub>. The model, which supports a large domain of conditions encountered in Low Earth Orbits (LEOs), was applied here in a thermosphere region where the main components are the four aforementioned ones in various percentages, with additional information on the total atmospheric density in selected altitudes taken from the NRL-MSISE-00 code [22]. This allowed to obtain data pertaining, e.g. to altitudes within 160 to 240 km, which are necessary for VLEO missions evaluation. Data that results from 4CDGM calculations, concerning the typical case of low and mean Solar and Geomagnetic (S&G) activities are illustrated in Fig. 2. Analogous data for high and very high activities as calculated by 4CDGM are provided in [22]. The S&G activities are described in terms of the 10.7 cm solar radio flux index  $F_{10.7}$  and the magnetic  $A_p$  index. The mean values were chosen as  $F_{10.7} = 140$ ,  $A_p = 15$ , low values as  $F_{10.7} = 70$ ,  $A_p = 8$  and high values as  $F_{10.7} = 250$ ,  $A_p = 100$ .

Figure 2 also includes results from the MSISE-90 code made available previously [23]. The latter were used in early ram-EP study by Di Cara et al. [24]. The data from Picone et al. [22] are also included. It can be seen from Fig. 2 that, for mean S&G activities, the values of the MSISE-90 code (constituting the best results available before 2000) are in good agreement with those coming from NRL-MSISE-00 and 4CDGM codes, except for O and N concentrations at altitudes below 190 km. At altitude above 190 km, all models agree well. Relative ratios of the number densities for the main constituents of the atmospheric remnants were given in [18] and are plotted in Fig. 2 for high solar activities. It is evident that variations of species other than N<sub>2</sub> and O have only a limited influence for the target altitudes. Lastly, Fig. 2 also provides a direct comparison among total number densities expected during low, mean, high, and very high solar activities

In the performed analysis, we focused on variation of atmospheric properties occurring during timescales shorter than a solar cycle. Even if long-term variations can be relevant, already along a single orbital period atmospheric flow properties varies significantly. For a dawn dusk SSO orbit, total number densities variation can be up to  $\pm 50\%$ . Concerning the flow composition accepted into the thruster, it is expected that higher utilization efficiency would be achieved with molecular N<sub>2</sub> and O<sub>2</sub> species, mainly due to their larger ionization



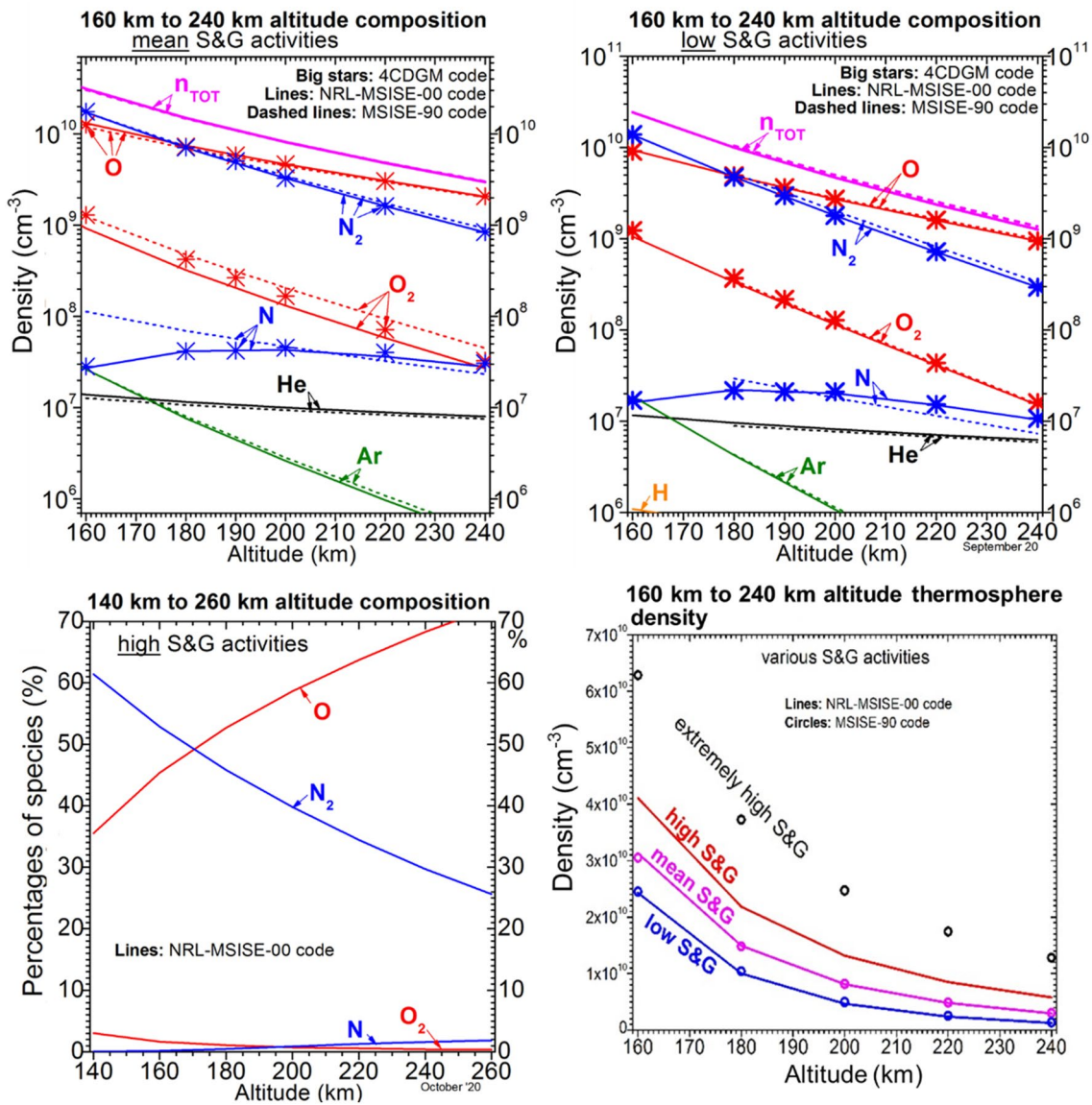


**Fig. 2** Earth atmospheric remnants for mean S&G activity (top-left) and low S&G activity (top-right), including comparison among 4CDGM, MSISE-90, NLRMSISE-00 atmosphere models. Bottom

figures show main species density ratios during high solar activities (bottom left) and comparison among total number densities during low, mean, high and very high solar activity (bottom right)

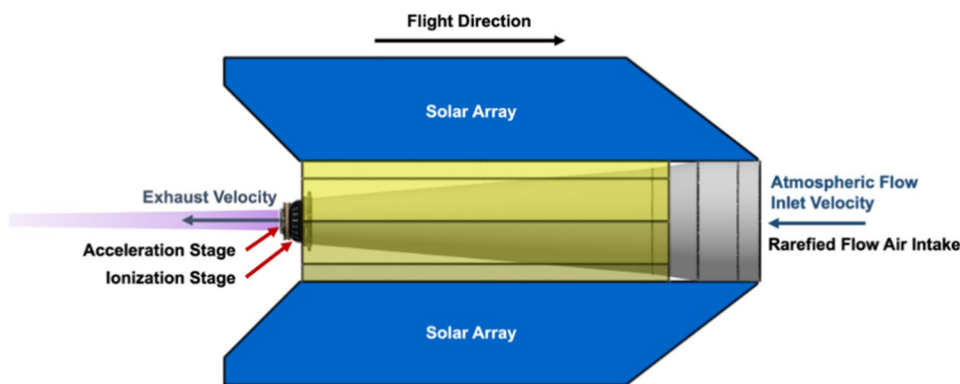
cross-sections together with their reduced thermal velocity (thus increased residence time in the thruster control volume) as compared to N and O atoms. As discussed in Sect. 6, atmospheric gases can only be stored in molecular form, which pose a limit to the on-ground verification capability of air-breathing systems. On the other hand, the presence of charged particles in the upper atmosphere is not expected to impact thruster performance due to typical low ionization degree ( $< 1e-4$  according to MSISE00). Nonetheless, as already mentioned, special attention shall be put in spacecraft grounding consideration and on mitigating the risk of potential arcing phenomena among the spacecraft components.

## 2.4 Requirement on air-breathing system performance

To design an end-to-end air-breathing propulsion system capable of providing full drag compensation, we considered a system, as visualized in Fig. 3, that comprises the following components:

- A rarefied flow air intake, having the function of collecting and passively compressing the inlet atmospheric flow; it also allows for low-drag payload and other platform sub-systems integrations behind its wake.

**Fig. 3** Schematics of the AETHER propulsion system



- An ionization stage, having the function of ionizing the flow gathered from the intake, channeling it toward the acceleration stage.
- An acceleration stage, having the function of accelerating the particles gathered from the ion stage to high exhaust velocity so to produce thrust.
- A Power Processing Unit, with the function of providing power to the system electrical loads and of controlling system operation and telemetry.

Even if the airbreathing EP concept seems relatively straightforward, the performance required to provide full drag compensation is demanding.

In VLEO, the flow regime is highly rarefied and particle motion is dominated by wall collisions. As such, is not rare for a particle entering the intake to just bounce back to the external environment without being accepted into the thruster. Defining the net thrust  $T_N$  produced by the ram-EP system as the resulting momentum variation over the entire propulsion system control volume, we see that four kind of particle populations contribute to the net thrust: (i) neutral particles entering the intake inlet at orbital velocity  $u_\infty$ ; (ii) neutral particles not accepted into the thruster and escaping back to the external environment through intake inlet at wall-thermalized velocity; (iii) neutral particles accepted into the thruster but not ionized and simply effusing to the external environment through the acceleration stage exhaust; (iv) ions accelerated to high exhaust velocity through the acceleration stage. Defining now the system collection efficiency  $\eta_c$  as the ratio between particle flux accepted into the acceleration stage,  $\dot{m}_{out}$ , and particle flux incident to intake inlet area,  $\dot{m}_{in}$ ; the effective exhaust velocity  $u_e$  as the momentum flux through the acceleration stage divided by the processed mass flowrate; and the effective inlet velocity  $u_{\infty,e}$  as the momentum flux through intake inlet area divided by incident mass flowrate, the thrust produced is expressed as

$$T_N = \dot{m}_{in} (\eta_c u_e - u_{\infty,e}), \tag{1}$$

where  $\dot{m}_{in} = \sum_s M_s n_{s,\infty} u_\infty A_{itk}$  is the n\_parainlet mass flow-rate, with  $M_s$  and  $n_{s,\infty}$  indicating respectively the molecular mass and number density of the  $s$  atmospheric constituent and  $A_{itk}$  indicating the intake inlet area. From Eq. (1), we see that the propulsion system can provide a positive net thrust only if the condition

$$u_e > U_e = \frac{u_{\infty,e}}{\eta_c} \sim \frac{u_\infty}{\eta_c}, \tag{2}$$

is met. For VLEO circular orbits, the orbital velocity  $u_\infty$  is of about 7.8 km/s. Depending on the achievable  $\eta_c$ , an exhaust velocity on the order of 10 km/s to 100 km/s is required. This range of exhaust velocity is commonly achieved by electrostatic devices which are now a mature technology counting on hundreds of successful flight applications [25]. For this reason, in the following the design of ram-EP thruster considers electrostatic acceleration. In the framework of the AETHER project, two different mechanisms have been considered for the thruster acceleration stage, corresponding to two well-known EP concepts, the Hall thruster and the Gridded Ion Engine (see Sects. 4.2 and 4.3, respectively). Despite the technological maturity of these acceleration mechanisms, the main challenge of electrostatic acceleration is related with the need of a cathode/neutralizer able to work with atmospheric propellant (see Sect. 5).

Notice that the net thrust, defined by Eq. (1) in the typical way of air-breathing engines, should compensate the drag  $D_{plt}$  produced by the spacecraft external surfaces, since the internal intake drag  $D_{itk}$  is already accounted for in the net thrust definition. A first analytical evaluation of the spacecraft drag can be performed by considering a GOCE-like architecture [26] and the model of Schaaf and Chambre [27]. These preliminary results have been consolidated by means of dedicated DSMC numerical simulations (see Sect. 3.2), resulting in equivalent platform drag coefficient in the 2.5 to 3.5 range depending on flow properties. Accordingly, Table 2 provides the high-level requirements derived for the propulsion system.

**Table 2** High level AETHER propulsion system requirements, see [28]

Mass	< 75 kg
Power consumption	1–2 kW
Net thrust	6–20 mN
Accelerator Isp	> 4000 s
Collection efficiency	> 0.2
Operating inlet flow number density	$3e15$ – $3e16$ m <sup>-3</sup> (190–240 km of altitude)

## 2.5 Mission analysis

According to the preliminary platform design identified in Table 1, the sum of S/C body projection toward solar flux direction and solar wing area is in the order of 11 m<sup>2</sup> which, depending on solar cells arrangement and efficiencies, should allow for a power generation in the 2 to 3 kW range by assuming an available power to solar flux efficiency between 14 and 20%. Considering continuous thruster operation and the expected power needed to provide full drag compensation, up to 1.5 kW are allocated to the propulsion sub-system while a minimum of 500 to 1000 W (depending on final payload selection) is allocated to payload and other platform subsystems. This resulted from a preliminary trade-off among typical power requirements of EO payloads and drag generated by a larger solar array area. For this first mission analysis, the PPU control loop (targeting a constant discharge power by acting on the thruster electrode voltage) described in Sect. 2.2 was not implemented, and the thruster was simulated as operating at a constant 600 V of acceleration voltage. The output of the analysis itself suggested that the implementation of such a control may be beneficial from the operational point of view, and more refined analysis implementing such a control will be performed in the next phase of the project. Relying on the assessment of atmospheric properties and on the thruster performance model described in [14], it was possible to preliminary evaluate the drag experienced by a GOCE-like spacecraft, the thrust produced by the RAM-EP thruster at a constant acceleration voltage of 600 V, as well as the power required by the propulsion system with respect to the maximum one allocated. The latter one defines how much of the available power is required by the propulsion system to fully compensate the atmospheric drag. A power fraction of 100% can be used to define a minimum altitude of the spacecraft for full drag compensation with maximum throttle. Below this minimum altitude the solar power is insufficient for full drag compensation and simultaneous operation of the payload. For medium solar activity, a minimum altitude of 198 km over the equator was found. In case of low solar activity, it is reduced to 194 km and for high solar activity it increases

to 209 km. It must be noted that these values are the altitudes where the complete available solar power is used by the thruster. If, for example, only 75% of the available power is foreseen for the thruster, because 25% of the power is reserved for spacecraft maintenance and payload operation, the minimum altitude increases to 209 km for medium activity level as well as 204 km and 222 km for low and high solar activity, respectively.

On the other hand, a maximum altitude where full compensation of the atmospheric drag is possible can be defined as well for the air-breathing engine. Since in higher altitudes, the density of the atmosphere is decreasing, the mass flow rate of the engine becomes smaller. In such case, due to lower air density and therefore flow rarefaction, the ionization of the flow particles becomes poor, and the engine loses efficiency. Considering a medium solar activity, a maximum altitude of about 211 km was found where full drag compensation is still possible. In case of low solar activity levels this altitude is reduced to 206 km, and for high activity it increases to 223 km. In summary, the altitude range where the air-breathing engine can be operated with full atmospheric drag compensation is defined by the available solar power (lower limit) and atmospheric density (upper limit), see Fig. 4. In principle both limits are based on the atmospheric density, since higher densities require more power than available to accelerate the increased mass flow rate, whereas lower densities cause inefficiencies in the flow properties of the ram-EP. Unfortunately, this altitude range is quite narrow: in case of medium solar activity, it is between 198 and 211 km, just 13 km difference. Low or high solar activity shifts this nominal altitude band either few kilometers down or up, respectively.

There is a criticality about this quite narrow altitude band in case of an SSO: the natural change in altitude due to the oblateness of the Earth (considering the influence of J<sub>2</sub>) is about 20 km [29], which is more than the nominal range where the engine can fully compensate the atmospheric drag. Since the altitude increases with higher latitudes, an orbit with an altitude over the equator close to the lower limit can be selected. However, when the spacecraft is next to the poles, the altitude is already more than the upper limit and the thrust magnitude can only partially compensate the atmospheric drag. Since this happens two times per orbit at opposite orbital positions, the orbital eccentricity cannot be maintained and slowly increases. This is even the case if the average thrust to drag ratio over one orbital revolution is 1 or higher. This behavior can be addressed by the definition of a proper control law for the thruster operation, for instance one based on mean orbital elements and aiming to prevent the thruster from firing around the orbit periapsis [15]. Performed simulations reveal that such control law is effective in establishing a long-term stable operating altitude for a dawn–dusk SSO.



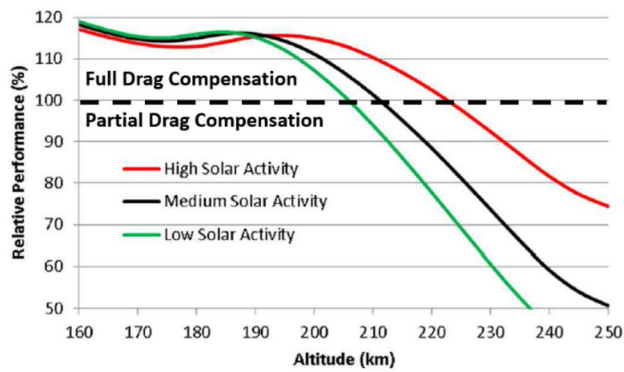
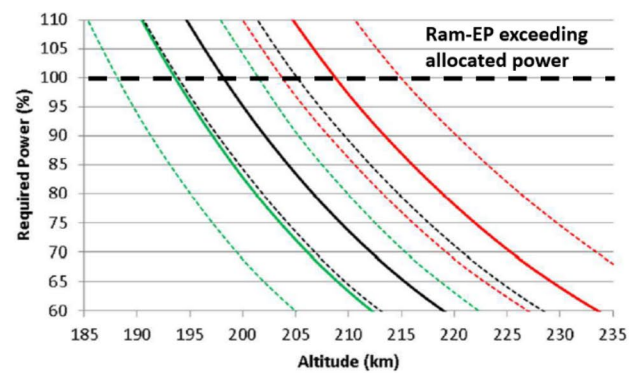


**Fig. 4** Left: average thrust-to-drag ratio, comparing the impact of low, medium, and high solar activity. Right: fraction of propulsion system power consumption vs allocated power as a function of the orbital altitude for different solar activities. Dashed lines represent

For instance, when modelling time-varying solar activity during a period of medium intensity, this results in an instantaneous periapsis-apoapsis range of around 10 km and total altitude range of around 25 km over a 500-day propagation.

Further relevant findings of the mission analysis are related to eclipses. It is known that sun-synchronous orbits have minimum eclipse durations when the orbital nodes are placed close to the terminator of the Earth. In such case the preferred local time of the ascending node (LTAN) is 6 p.m. in case of a dusk-dawn orbit and 6 a.m. in case of a dawn-dusk orbit. However, such orbits still encounter two eclipse seasons per year with a total eclipse maximum duration of up to 30 min. Considering partial eclipses as well increases the maximum eclipse duration to 45 min, corresponding to 50% of the orbital period. Besides, eclipses exist at 59% of the days per year. Thus, another criticality is the availability of solar power. Since we are assuming that the air-breathing engine is continuously operated, high battery capacity is mandatory. More solar power is required to charge the battery, potentially increasing the aerodynamic drag.

In case, the orbital nodes of the SSO are not placed close to the terminator, there are two drawbacks for the mission concept and especially the power budget. First, the total eclipse duration increases to  $\varphi$  min for a noon-midnight orbit. Since there are no eclipse seasons in such orbit, the eclipse duration is constant over the year. With a local time of ascending node of either 5 p.m. or 7 p.m. the maximum total eclipse duration is 31 min. Such orbits feature almost the same eclipse behavior as the terminator SSO. The second drawback is related to the alignment of the solar arrays. Because the Sun is not perpendicular to the orbital plane anymore, the solar arrays cannot be kept parallel to the velocity vector to generate the required solar power. This increases the cross-section area of the spacecraft and thus



impact of flow properties variation along the same SSO orbit on the plotted performance. For both figures, the accelerator voltage is fixed at 600 V (no PPU control loop on discharge power implemented)

the atmospheric drag. The system impact is huge due to the large arrays with respect to the spacecraft body (i.e., intake).

### 3 Rarefied flow air intake and platform aerodynamics

#### 3.1 Intake design optimization

Based on the preliminary platform requirements of Table 1, the design of the intake was performed aiming at the optimization of the particle collection and of the flow passive compression. The core components of the optimization system are a single-, or multi-objective Differential Evolution (DE) algorithm, a database, several metamodels, and a high-fidelity evaluation chain [30], which comprises a fully automatic geometry and CAD generation and a View-Factor Based Panel Method (VFM) SMARTA [31], which was developed as an alternative to Monte Carlo particle methods for free molecular flows with diffuse reflections.

The optimization based Evolutionary Algorithms (EA), is explained as the evolution of individuals through generations, and subjected to genetic operations like mutation, cross-over, and selection, and at the end the fittest survives. For the intake optimization, we considered 1000 generations of 50 individuals each. A total of 50,000 designs ( $50 \times 1000$ ) must be evaluated which is only feasible by a metamodel, which is trained with an initial 128 case database created with the Design of Experiment method using SMARTA at the beginning of the optimization. This metamodel is retrained after each iteration with the new database where the hi-fidelity VFM solution of the optimal design from the last iteration is added, [32]. The intake geometry is fully parametrized with 10 design variables, a CAD geometry is automatically produced which is meshed with open source GMSH [33], and the fitness is evaluated with SMARTA. The

selected intake design variables include intake inlet radius, number of inlet ducts, length of the duct section, length of the intake conical section, lengths of two cylindrical sections upstream and downstream the conical portion of the intake, inlet and outlet sweep angle of the inlet ducts with respect to the intake axis, and inlet channel slant angle, see Fig. 5.

The optimization is performed for the 190 km sun synchronous orbit (SSO) at medium solar activity conditions, at satellite speed of 7794 m/s, for fully collimated 50–50%  $N_2/O$  composition gas flow at 778 K with total density of  $8.26 \cdot 10^{15}$  particles/m<sup>3</sup>. We assumed a fully accommodated surface is at 300 K. While in principle purely reflective parabolic shape would result in maximum performance, we choose cylindrical and conical shapes for their intrinsic simplicity of realization, while the wall accommodation was

set to 1 as most materials used in practical applications are highly diffusive. An altitude of 190 km was selected as a reference as it represents the minimum expected operating altitude of the system. In this regard, optimizing the overall platform design at minimum operating altitude has the advantage of optimizing at maximum expected drag conditions while ensuring increasing performance (e.g., in terms of thrust over drag ratio) with decreasing operating altitude, in principle allowing for an intrinsic stability in platform orbit maintenance. Intake performance sensitivity analyses to different altitudes, wall temperatures and accommodation are currently being performed for the optimal design selected, see Table 3.

The main performance variables of the intake are the collection efficiency,  $\eta_c$ , and the compression ratio  $\nu$ , which

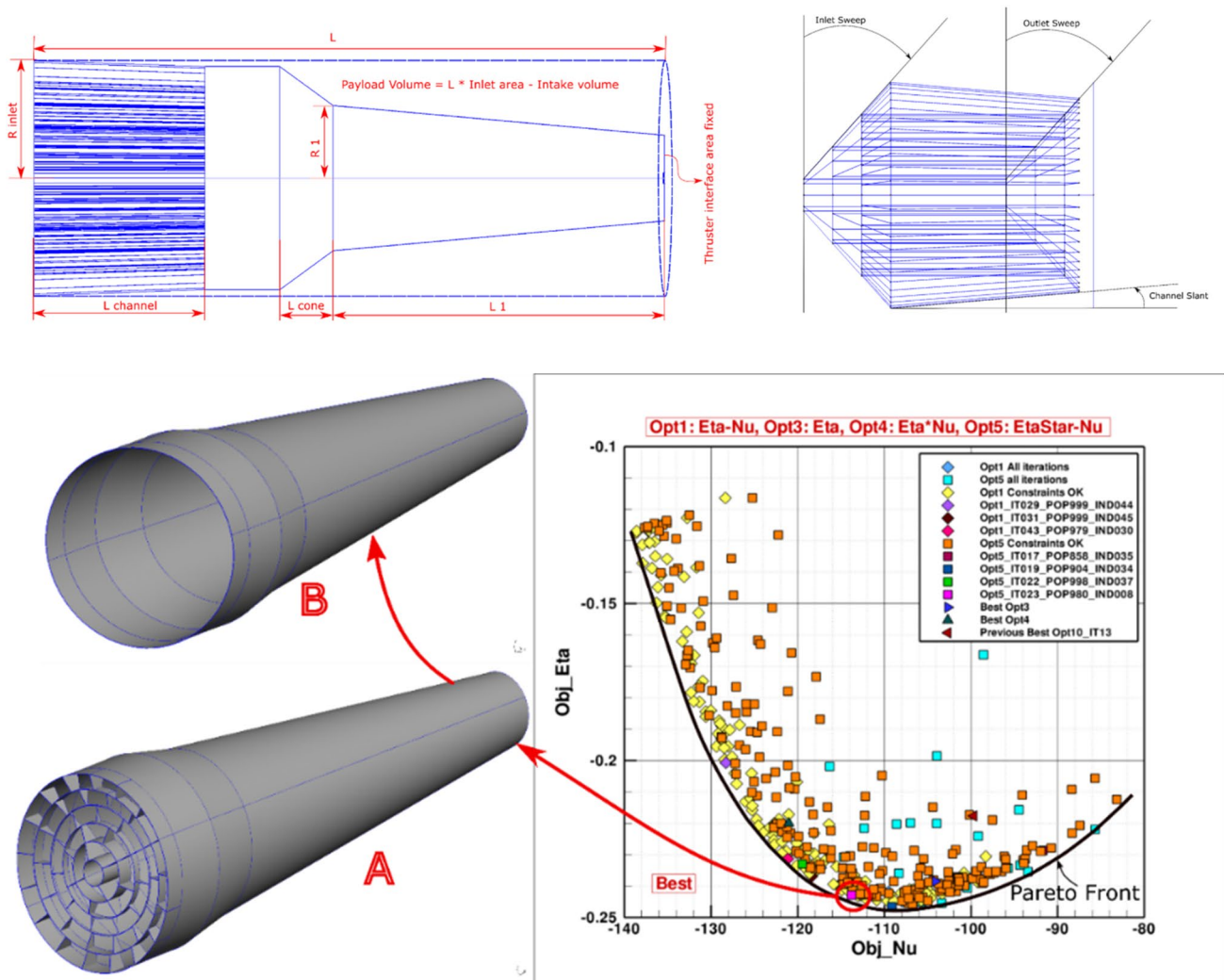


**Fig. 5** Top: Intake optimization design parameters. Bottom: Initial best candidate as optimization result with channels. According to another optimization performed for geometries without channels, geometry A without channels (i.e., geometry B) was confirmed as

optimal for weight, total length, and collection efficiency. The hypothetical Pareto Front is depicted for illustration purposes. The legend refers to the different optimization codes used

**Table 3** Sensitivity to environmental conditions and thruster transparency variation, VFM solutions. Here,  $I_{sp,min} = D_{itk} / (g_0 \dot{m}_{out})$  is the minimum specific impulse that the thruster shall provide to have a positive net thrust, with  $g_0$  the gravitational acceleration

Cases	$\eta_c$	$v$	$\eta_c \cdot v$	$D_{itk}$ [mN]	$\dot{m}_{in}$ [mg/s]	$\dot{m}_{out}$ [mg/s]	$I_{sp,min}$ [s]
Design*	0.251	116.7	29.28	15.78	2.002	0.502	3204
$T_{WALL}=213$ K	0.251	138.5	34.75	15.69	2.001	0.502	3187
$T_{WALL}=473$ K	0.251	92.96	23.31	15.90	2.001	0.502	3231
$T_{\infty}=646$ K	0.257	118.7	30.53	15.46	2.001	0.515	3063
$T_{\infty}=1053$ K	0.238	112.5	26.80	16.40	2.001	0.477	3507
$V_{\infty}=7692$ m/s	0.250	114.9	28.70	15.41	1.975	0.493	3186
$V_{\infty}=7935$ m/s	0.252	119.3	30.06	16.27	2.037	0.514	3230
$N_{TOT}=0.4 \cdot 10^{16}$	0.251	116.7	29.28	7.64	0.969	0.243	3204
$N_{TOT}=1.7 \cdot 10^{16}$	0.251	116.7	29.28	32.45	4.118	1.033	3204
$N_{N_2}/N_O=4$	0.256	128.6	32.93	18.01	2.329	0.597	3078
$N_{N_2}/N_O=0.4$	0.246	108.3	26.62	14.17	1.767	0.434	3327
YAW = 3.0 DEG	0.240	113.3	27.16	16.27	2.002	0.480	3455
YAW = 3.6 DEG	0.235	111.7	26.25	16.48	2.001	0.470	3572
$A_{THR}=25\%$	0.133	188.1	25.08	15.73	2.002	0.267	6008
$A_{THR}=25\%$ & YAW = 3.0 DEG	0.127	181.6	23.14	15.90	2.002	0.255	6481

\*Design conditions are  $T_{WALL}=300$  K,  $T_{\infty}=778$  K,  $V_{\infty}=7794$  M/S,  $N_{TOT}=0.826 \cdot 10^{16}$ ,  $N_{N_2}/N_O=1$ , YAW = 0 DEG,  $A_{THR}=75\%$

is the ratio between the intake outlet and inlet number densities. The design considered a 75% thruster transparency, which should be representative of the resistance to the approaching particles of the thruster in ON condition thanks to ionization and ion channeling processes for which the ionization stage is designed for. Lower values of thruster transparency below 10% are expected when in OFF condition. The thruster transparency  $\alpha_{thr}$ , also called transmission, is defined as the ratio between particle flux accepted into the acceleration stage and particle flux collected from the intake at ionization stage inlet area. Sensitivity of intake performance on thruster transmission is provided in Table 4 for  $\alpha_{thr}=75\%$  and  $\alpha_{thr}=25\%$ . The drag due to the intake internal surfaces changes of around 30% when the engine is switched ON/OFF. At platform level, this implies a drag increase in the 10–15% range when the thruster is OFF. Combined with intake transmission  $\alpha_{itk}$ , we can define the overall system collection efficiency as

$$\eta_c = \alpha_{itk} \alpha_{thr} \tag{3}$$

Both intake and thruster transmission are sensitive to inlet flow composition, temperature, orbital velocity, on/off status of the thruster, and spacecraft attitude.

We have used single-objective (SO) optimization, formed with weighted sum of the performance variables  $\eta_c$  and  $v$ , as well as multi-objective (MO) optimization, with a separate objective function for each performance variable. MO has the advantage of allowing the assessment of each objective separately, but they are more expensive and more difficult to interpret because the result, as illustrated in Fig. 5, is a so-called Pareto front for each pair of objective functions, which is the set of nondominated solutions. Each design on a Pareto front is an optimal design which cannot be improved without sacrificing at least one objective. For each optimization iteration, six individuals with equal spacing along the Pareto front were analyzed and added to the database,

**Table 4** Sparta DSMC and SMARTA VFM comparison of the flow properties at the exit of the intake for 25% and 75% thruster transparencies and freestream design conditions ( $n_{tot}=0.826 \cdot 10^{16}$ ,  $n_{N_2}/n_O=1$ )

CASES	$N_{N_2}$ [M <sup>-3</sup> ]	$N_O$ [M <sup>-3</sup> ]	$v_{N_2}$ [-]	$v_O$ [-]	$v$ [-]		$D_{itk}$ [MN]		$\dot{m}_{out}$ [MG/S]	
					SPARTA	SMARTA	SPARTA	SMARTA	SPARTA	SMARTA
$A_{THR}=75\%$										
No-coll	$3.84 \cdot 10^{17}$	$2.80 \cdot 10^{17}$	93	68	80	117	15.67	15.78	0.50	0.50
Collision	$3.75 \cdot 10^{17}$	$3.71 \cdot 10^{17}$	91	66	78		16.10		0.46	
$A_{THR}=25\%$										
No-coll	$8.03 \cdot 10^{17}$	$5.70 \cdot 10^{17}$	195	138	166	188	15.34	15.73	0.26	0.27
Collision	$7.51 \cdot 10^{17}$	$5.37 \cdot 10^{17}$	182	130	156		15.93		0.24	

making the system more expensive but more efficient, thus converging faster. The optimization minimized the collection efficiency  $\eta_c$  and compression ratio  $\nu$  which constitutes (with a negative sign) the axes of the Pareto front in Fig. 5.

The design constraints imposed were (i) intake weight with 1 mm wall thickness, 1200 kg/m<sup>3</sup> Al alloy material < 40 kg; (ii) Minimum 0.2 mg/s thruster intake mass flow; (iii) Payload volume behind intake wake > 1.5m<sup>3</sup>. The launcher-imposed envelope was 1.6 m diameter and 4.5 m length. A collection efficiency > 25% and compression ratio > 100 were desired. The design constraint on available intake wake volume resulted from a very preliminary assessment of main platform subsystems envelopes, including a 20% margin. In general, reducing the requirement on wake volume improves intake performance, and optimal intake designs may be defined as the ones minimizing the requirement on minimum thruster exhaust velocity given the platform constraint on wake volume.

A series of optimizations led to noticeably short intake channel best candidate, in view of 4 m total intake length, intake channels were not highly effective. Indeed, flow properties inside the thruster control volume are mainly influenced by the equivalent aspect ratio of the intake given the inlet flow collimated velocity over thermal speed ratio. For sufficiently long intake envelopes, which allow for an increased payload volume available behind the wake, ducts are detrimental due to additional drag caused by the duct lateral surface. On the other hand, ducts are beneficial for

shorter intake shapes to increase the effective aspect ratio of the funnel. Further geometric sensitivity analysis of  $\pm 10\%$  of the design variable range revealed that an intake without channel is better suited. An additional no-channel optimization confirmed the optimality of the other design variables as obtained from the previous optimization. A thorough sensitivity analysis also on the environmental conditions and thruster transparency using SMARTA has proven the good performance of the intake, Table 3. Comparisons of the VFM with the open-source SPARTA Direct Simulation Monte Carlo (DSMC) calculations to verify the design are shown in Table 4.

### 3.2 Aerodynamic assessment of a Ram-EP platform

As a first step to integrate the designed intake into a platform, a GOCE-like architecture was selected [26]. This design was only meant to be a tentative first shape to estimate the aerodynamic forces acting on the satellite for trajectory calculations, as well as for the thruster design, Fig. 6. As the next step to the platform design, numerical activities with the VFM and DSMC are currently on-going to aerodynamically optimize the platform, as it was done for the intake.

DSMC computations with SPARTA on a GMSH generated triangular surface mesh with 545,442 points and 181,814 triangles have been performed for 25% thruster transparency setting with and without collisions. First

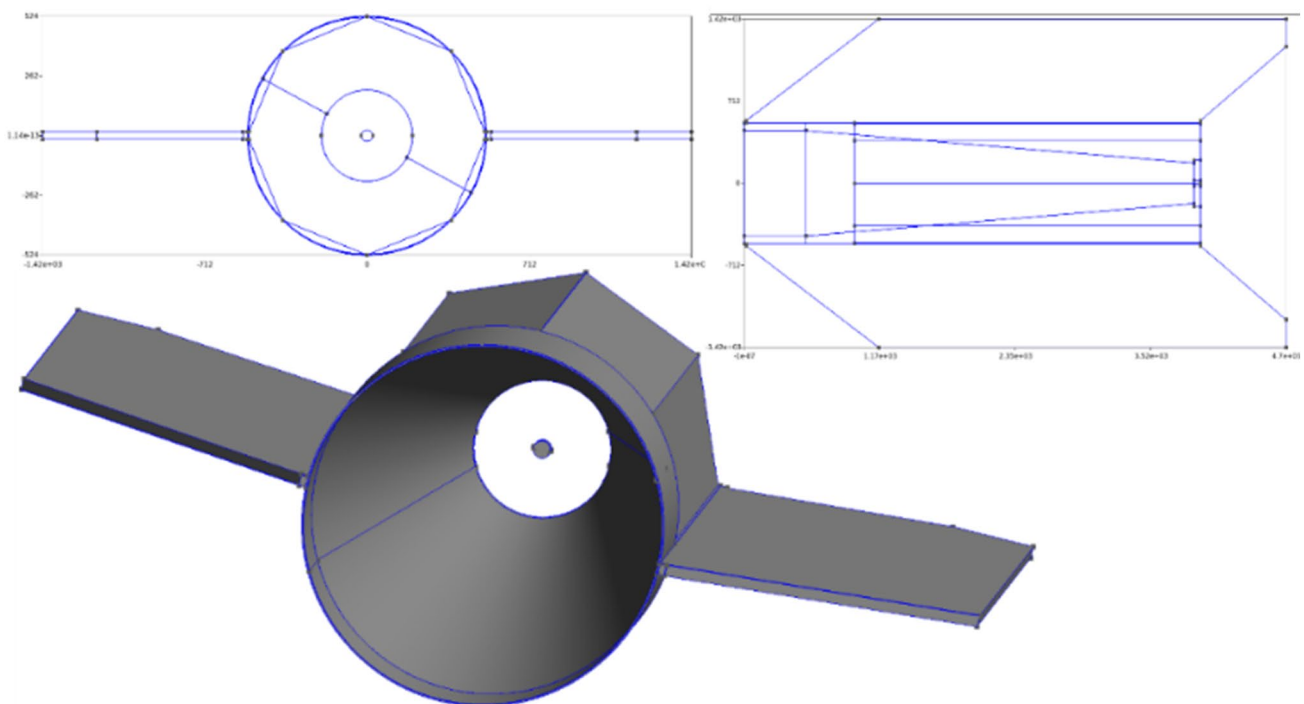


**Fig. 6** GOCE-like platform designed for the first intake-platform integration aerodynamic analysis



investigations are made at the intake design point: collimated flow at the same SSO medium solar activity orbital flight conditions. A summary of the calculations is given in Table 5.

An important conclusion that can be drawn from the standalone intake and platform calculations is that, besides the remarkable consistency of the results, the VFM SMARTA and DSMC without gas phase collision results compare well. Also, the DSMC results with and without collisions justify the assumption of free molecular flow under given orbital conditions. A 3D view of the flow field is shown in Fig. 7.

### 4 Air-breathing thruster: the AETHER concept

The main function of the air-breathing thruster is to ionize and accelerate the collected atmospheric particles to produce thrust. As described in Sect. 2.5, the ability of the thruster to effectively ionize the collected particles define the upper limit of feasible orbit altitudes. In Hall thrusters or gridded ion engines, neutral particles are typically injected with number densities  $\sim 10^{18}\text{--}10^{19} \text{ m}^{-3}$ . Considering that

atmospheric particles require more energy to be ionized with respect to traditional EP propellants (e.g., Xe and Kr) and that particle densities at the altitudes of interest are at least two orders of magnitude lower than in state-of-the-art thrusters, the air-breathing thruster developed in the framework of the AETHER project features a dedicated ionization stage. The ionization stage is designed to connect to the two different accelerator technologies, named as Closed Drift Accelerator Stage (CDAS) and Charge Separation Accelerator Stage (CSAS). A dedicated ionization stage sub-assembly, called CSAS Interface, allows for ionization stage compatibility with both accelerator technologies. Integration of the ionization stage in the overall ram-EP thruster assembly is shown in Fig. 8, which illustrates both the CDAS and CSAS based thruster configurations. More details on the CDAS and CSAS accelerators are provided in the following sections.

#### 4.1 Ionization stage

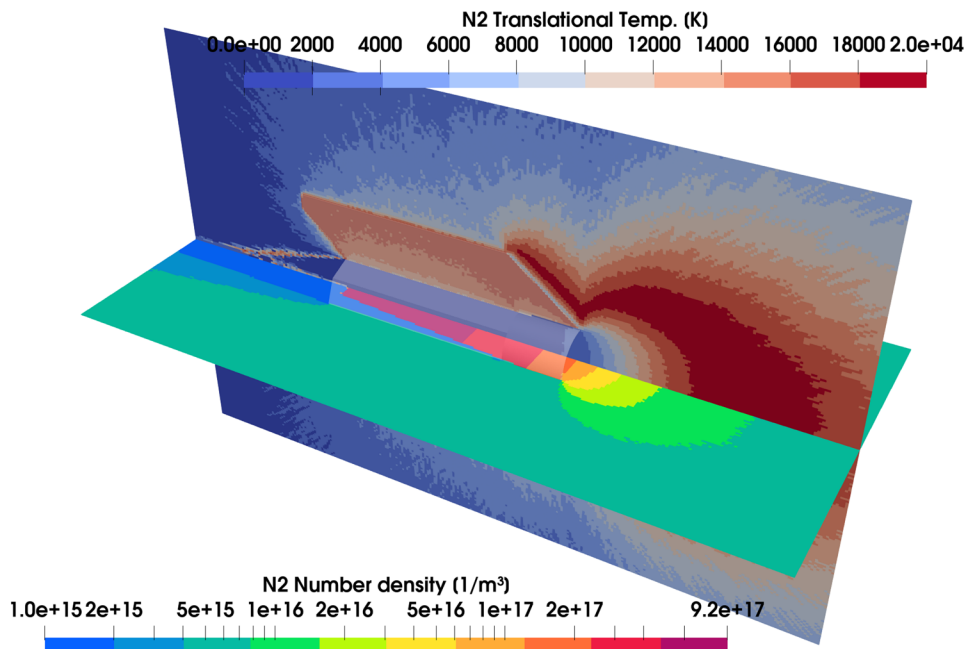
The ionization stage is the core of the AETHER propulsion system. It features a relatively large open inlet area designed to be connected to an air intake and to operate in air-breathing mode in VLEO environment. The ionization stage uses

**Table 5** DSMC Platform-Intake calculation results for the 25% thruster transparency and freestream design conditions ( $n_{tot}=0.826 \cdot 10^{16}$ ,  $n_{N2}/n_O=1$ ), with and without gas phase collisions. Here  $D_{tot}$

indicates the sum of platform and internal intake drag, which represents the target for the thrust produced by the ram-EP thruster in stand-alone condition (without the intake)

Cases		$N_{N2} [M^{-3}]$	$N_O [M^{-3}]$	$v_{N2} [-]$	$v_O [-]$	$v [-]$	$D_{itk} [MN]$	$D_{plt} [MN]$	$D_{tot} [MN]$	$\dot{m}_{in} [MG/S]$	$\dot{m}_{out} [MG/S]$
$A_{THR}=25\%$	No-coll	$7.95 \cdot 10^{17}$	$5.59 \cdot 10^{17}$	192	135	164	12.99	14.45	27.44	2	0.26
	Collision	$7.40 \cdot 10^{17}$	$5.25 \cdot 10^{17}$	179	127	153	13.26	14.79	28.05	2	0.24

**Fig. 7** 3D Flow around and through the platform. On the horizontal plane the density, and on the vertical plane the translational temperature of  $N_2$  is shown



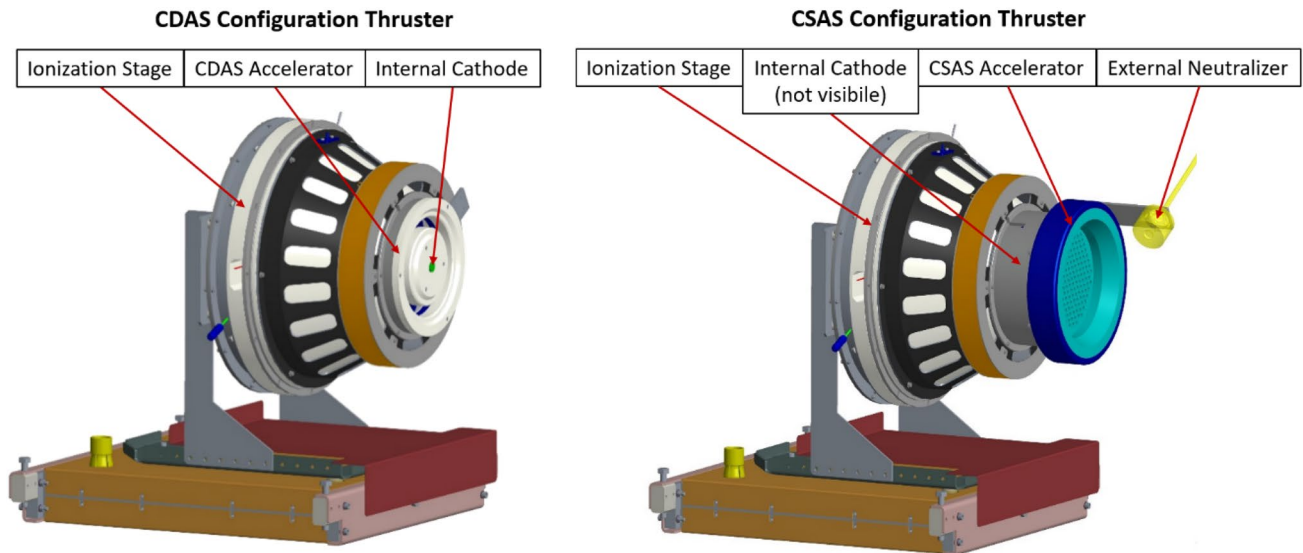


**Fig. 8** Ram-EP thruster installed on thrust balance for stand-alone testing. Left: CDAS configuration. Right: CSAS configuration. The ionization stage inlet is leak tight closed by means of a cover

available electrical power to ionize the compressed flow by electron impact. Its design is compatible with integration in both internal and external position of both hollow and RF pipe-fed cathodes, which provide the electronic current required to trigger the discharge and neutralize the thruster plume. An auxiliary propellant injector, located at the bottom of the stage, allows for stand-alone testing activities of the thruster assembly.

In this regard, the main ionization stage performance indicator is its capability to ionize and channel the inlet flow to the acceleration stage. The ionization stage performance is thus quantified by the thruster transmission  $\alpha_{thr}$ , defined as the ratio between particle flux accepted into the acceleration stage and particle flux collected from the intake at ionization stage inlet area. As for other well-known electrostatic devices, another performance indicator is the ionization stage current utilization efficiency  $\eta_{I,i}$ , here defined as the ratio between ion current channeled into the acceleration stage and discharge current flowing between ionization stage anode and acceleration stage intermediate electrode, from which the ionization stage discharge power is computed as

$$P_{D,i} = \frac{e(V_i - V_a)}{\eta_{I,i}} \sum_s \eta_{i,s} \alpha_{itk,s} \Gamma_{in,s}, \quad (4)$$

where  $V_i$  is the ionization stage anode electrode bias voltage with respect to the acceleration stage cathode,  $V_a$  is the acceleration stage electrode bias voltage,  $\eta_{i,s}$  is the fraction of propellant accepted into the ionization stage which is ionized, and  $\Gamma_{in,s} = n_{\infty,s} u_{\infty} A_{itk}$  is the inlet s-species particle flowrate.

mounted on the auxiliary injector mechanical interface (which is nominally used for intake mounting)

## 4.2 Closed electron drift accelerator

The primary function of the ram-EP thruster Closed Drift Acceleration Stage (CDAS) is to produce thrust by electrostatic acceleration of the particles collected from the ionization stage. The CDAS is basically composed of electromagnets, electrodes, and structural/insulating elements. Its design and principle of operation is equivalent to an open-inlet Hall thruster and relies on producing an almost radial magnetic field at the exit of the acceleration channel. The magnetic field peak at channel exit should allow for the formation of a self-consistent plasma potential drop which accelerates the ions. At the same time, electrons emitted from the cathode should make their way through the acceleration channel, arriving inside the ionization stage volume and ionizing by electron impact the neutral particles collected by the intake.

Depending on the acceleration voltage (the one at which the CDAS intermediate electrode is biased), the accelerator discharge power is computed by introducing the accelerator current utilization efficiency  $\eta_{I,a}$

$$P_{D,a} = \frac{eV_a}{\eta_{I,a}} \sum_s \eta_{i,s} \alpha_{itk,s} \alpha_{thr,s} \Gamma_{in,s}, \quad (5)$$

where  $\alpha_{thr,s}$  is the fraction of particle flow accepted into the ionization stage which is transmitted to the acceleration stage and  $\eta_{i,s}$  is the fraction of flow in the accelerator which is ionized. Moreover, the exhaust velocity achievable by the s-species can be expressed as

$$u_{e,s} = \eta_{div,s} \eta_{i,s} \tag{6}$$

where  $\eta_{div,s}$  accounts for thrust losses due to plume divergence and  $\eta_v$  is the voltage utilization efficiency. As such, the effective thrust efficiency  $\eta_{T,s}$  accounts for several thrust detrimental effects, such as incomplete propellant ionization, ineffective ion acceleration, unstable thruster-cathode coupling, and plume divergence.

Figure 9 shows the achievable exhaust velocity vs acceleration voltage and thrust efficiency. For thrust efficiencies higher than 50%, which is a typical value for state-of-the-art electrostatic devices, the criterion for providing a positive net thrust  $u_e > U_e$  can easily be met. Figure 9 also shows the behavior of  $u_e/U_e$  vs acceleration voltage and overall air-breathing thruster performance  $\alpha_{thr} \eta_T$  for an  $\alpha_{itk} = 0.25$  intake transmission, representative of our reference design. Considering 0.25, 0.5 and 0.75 as reference values for  $\alpha_{thr} \eta_T$ , only acceleration voltages higher than 2000 V, 450 V and 250 V, respectively, can provide positive net thrust. Even if achieving sufficiently high thruster performance with atmospheric propellant is not obvious, acceleration voltage levels in the 300 V to 3000 V range are commonly used by electric engines operating with Xe

### 4.3 Charge separation accelerator

The CSAS is an electrostatic accelerator composed of electrodes set onto the holders, insulators/spacers, a mechanical structure/interface towards ionization stage, and electrical interfaces: screen grid high voltage connector, accelerator grid high voltage connector.

The CSAS design consists of three electrodes grid system (number 4 at Fig. 10) and the flange to mechanically support the electrodes and interface the CSAS to the ionization stage. Every electrode is composed of a flange with an attached thin perforated plate. The first screen

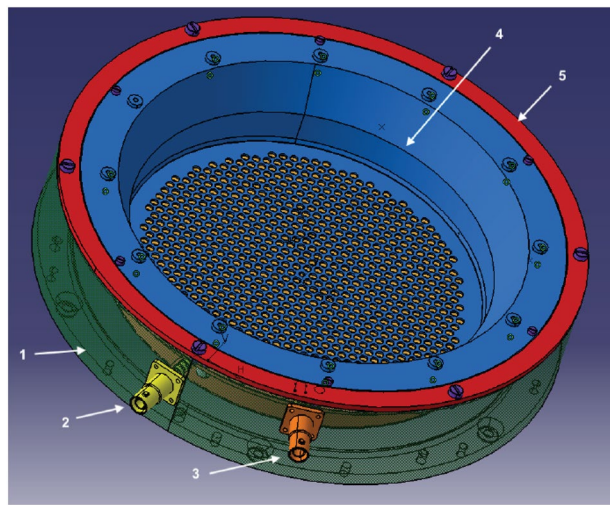


Fig. 10 CSAS 3D assembly

electrode and the second accelerator electrode allocate pin connections where the high voltage connectors are to be attached, the third deceleration electrode should be then connected to the power supply and/or common system ground by the ring crimp connection screwed on to it. Screws are also used to mechanically attach the grid system sub-assembly to the CSAS flange. The electrodes are assembled into the grid system package by means of isolation packs.

The CSAS flange sub-assembly consists of a flange itself (number 1 at Fig. 10) with connected to it SHV connectors used to supply positive (number 2 at Fig. 10) and negative (number 3 at Fig. 10) high voltage to the electrodes of the grid system and additional electrically isolating ring (number 5 at Fig. 10). That ring is introduced between the flange and the grid system sub-assembly allowing setting different potentials to the third grid

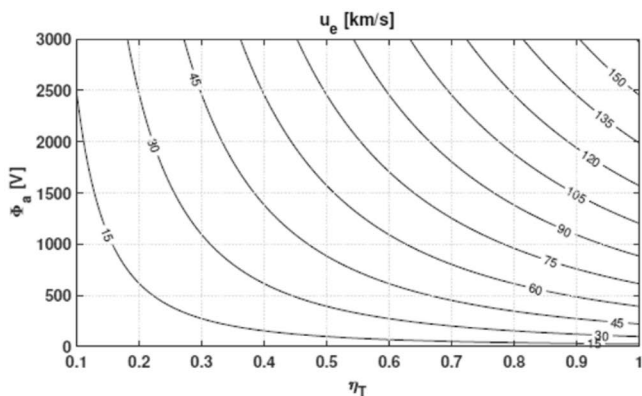
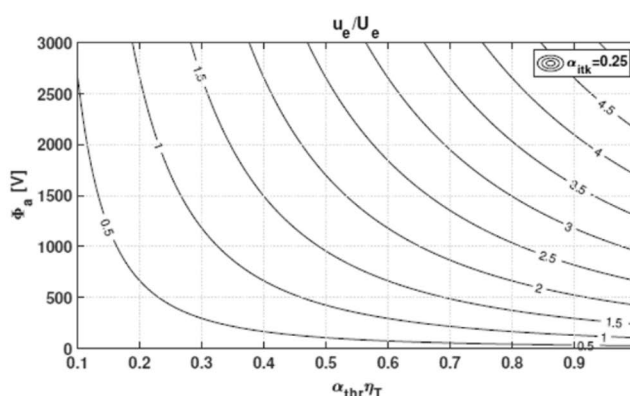


Fig. 9 Left: achievable exhaust velocity  $u_e$  vs acceleration voltage and thrust efficiency. Right:  $u_e/U_e$  vs acceleration voltage and thruster performance, for a reference 25% intake transmission.  $U_e$  is computed



according to Eq. 2, while  $u_e$  is computed by Eq. 6 by considering an effective  $M_\infty = 21$  amu mean propellant mass (representative of mean VLEO composition at 200 km of altitude)

and the CSAS flange to comply with the requirement on variability of electrical schemes in terms of grounding of the full RAM-EP system.

The exhaust velocity generated by the CSAS is given in general by

$$u_{e,s} = \eta_{\text{div},s} n_{i,s} \sqrt{2e\eta_v(V_a + V_p)/M_s}, \quad (7)$$

where  $M_s$  is the mass of ionic species  $s$ ,  $V_a$  is the positive high voltages,  $\eta_{\text{div}} = 0.96$  represents the divergence efficiency, and  $V_p$  is the plasma potential in the plume. The power consumption  $P$  of the thruster may be written as the sum of all individual contributions:

$$P = I_a V_a + I_d V_- = I_a (V_a + \beta V_-) \quad (8)$$

where  $I_a$  is the extracted ion current,  $I_d$  is the drain current and  $V_-$  is the negative high voltage of the intermediate grid. Note that  $I_d$  or  $\beta = I_d/I_a$  depends strongly on the pressure between the grids, because the drain current is caused mainly by charge-exchange processes. For the present activity, it is conservatively assumed to be 0.05. The realistic drain current ratio to total extracted current shall be verified by test. Total extractable current and thus beam current depends strongly on one hand on plasma parameters before the CSAS but on the other hand, it is limited due to the space-charge. Therefore, it might be not possible to

effectively extract all the available ions from the plasma of the ram-EP.

Clearly, experimental data will allow to refine the thrust/drag budget of the platform. As discussed in Sect. 3, the intake and platform aerodynamic assessment was performed at a reference of 190 km SS0 6-a.m. medium solar activity orbit, corresponding to minimum expected operating altitude, and thus maximum drag. Considering targeting a comparable acceleration power level for both the CDAS and CSAS configuration, and due to the higher acceleration voltages characterizing the CSAS accelerator, it is expected that their optimal operating altitude range (to be confirmed downstream experimental activities) will be slightly different. Approximating the intake collection efficiency, intake drag and platform drag as varying linearly with the inlet flow total number density, and considering a constant thruster transmission  $\alpha_{\text{thr}} = 0.8$ , we plot in Fig. 11 the expected qualitative behavior of intake/platform/total drag, mass flowrate incident to intake inlet area and collected to the thruster, and thrust produced by the CDAS and CSAS thruster configurations. In figure below, we assume the PPU to control the accelerator voltage to operate at a constant accelerator power of 1 kW, while about 750 W are allocated to the propulsion system auxiliary loads.

According to the current design, the CSAS operating envelope is constrained by the maximum ion current that can be extracted due to space-charge separation. On the other hand, we expect that the operating envelope of the CDAS

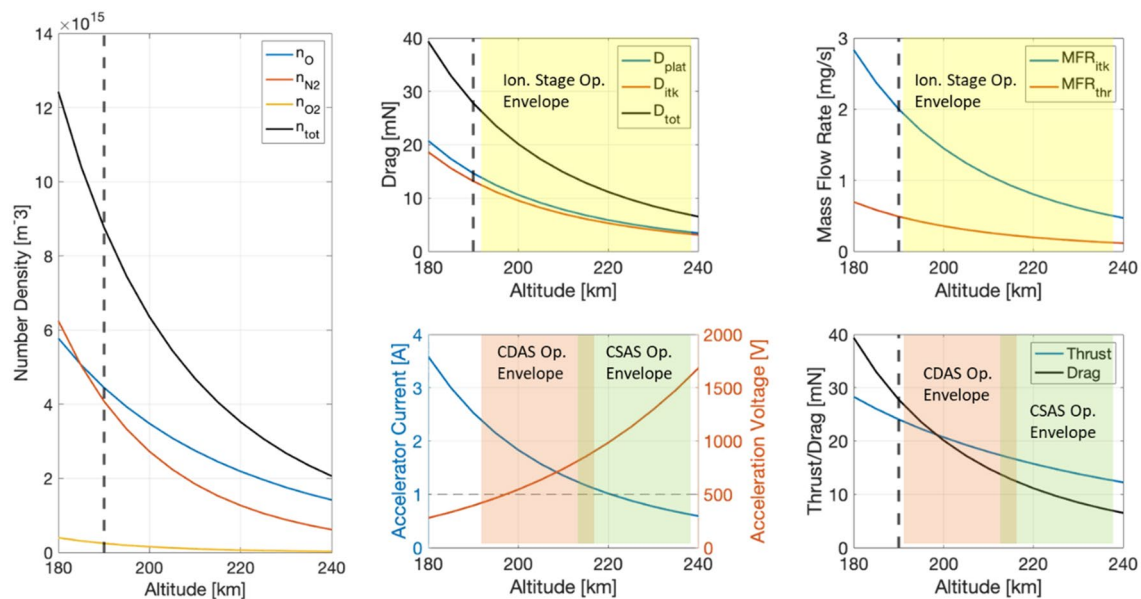


**Fig. 11** Atmospheric number density vs altitude (SSO 6am, medium solar activity); intake, platform and total drag vs altitude; incident intake mass flow rate and thruster mass flow rate vs altitude; CDAS and CSAS acceleration voltage and current vs altitude (assuming a constant 1 kW of accelerating power by PPU discharge control);

Thrust and total drag vs altitude (note that above 240 km of altitude the thrust would exponentially decay due to low propellant density and poor ionization efficiency). Indicative operating envelope for ionization stage, CSAS and CDAS accelerators are highlighted. A thruster transmission  $\alpha_{\text{thr}} = 0.8$  and thrust efficiency  $\eta_1 = 0.5$  are used



accelerator will be limited by the maximum acceleration voltage allowing for a stable discharge. As shown in Fig. 11, the higher operating voltages thus specific impulses achievable by the CSAS configuration allows achieving higher thrust over drag ratios, but constraints CSAS operation (due to the constraint on maximum extractable ionic current) to operate at higher altitude with respect to the CDAS configuration. Note that the trends and indications on operating envelope are only indicative and shall be confirmed by experimental data analysis.

## 5 Atmospheric propellant fed cathode development

### 5.1 Radio-frequency cathode/neutralizer

The alternative neutralizer is a microwave plasma electron source which, to the authors' best knowledge, is the first neutralizer developed for operation with air at conditions representative of VLEO. In the neutralizer, neutral propellant gas is introduced into an internal chamber with externally applied microwaves, where energy transfer occurs through wave-particle interaction. An electron current is extracted from the resultant high-density plasma due to a potential difference between the negatively biased ion-collecting electrode within the neutralizer and the positively biased thruster plume. The design approach includes a Molybdenum microwave antenna which is directly inserted into the plasma chamber to deliver a time-varying electric field into the plasma. The resulting ion current is collected by the negatively biased (or grounded) neutralizer chamber walls, allowing an equal electron current to be extracted out of the orifice whilst maintaining charge conservation within the neutralizer plasma. The chamber diameter is sized based on the area needed to sustain a predicted post-intake neutral density of  $5 \times 10^{18} \text{ m}^{-3}$  at the upper expected mass flow rate of 0.1 mg/s. The chamber length is determined by the area required for current collection, based on an estimate of the current density available at the sheath of the internal ion-collecting electrode.

The neutralizer development investigates the promotion of several mechanisms to increase the density and energy of electrons. One such mechanism is Electron Cyclotron Resonance (ECR), for which the design is based on the development of the JAXA  $\mu 10$  neutralizer [34]. The ECR principle involves an applied static magnetic field which induces a gyro frequency of the electrons matching the microwave frequency [35]. Electrons are efficiently heated due to absorption of microwave energy at the ECR resonant frequency of 2.45 GHz for a magnetic-field strength of 87.5 mT. A magnetic-field configuration designed to promote ECR is tested as part of the development, based on electron containment in

a magnetic mirror formed between points of high magnetic-field strength and centred around the antenna, where the maximum microwave-induced electric-field occurs. For testing purposes, the magnetic circuit is composed of either a Samarium Cobalt permanent magnet or electromagnet coil, which is coupled to guiding iron yokes. Secondary Electron Emission (SEE) is also investigated as part of testing, aiming at increasing the extracted current by means of electrons emitted from the internal neutralizer surfaces in contact with the plasma. The effect of varying magnetic-field magnitude and topology on electron current is analysed as part of the development testing, including on the promotion of ECR and SEE. From a spacecraft viewpoint and in the event that the neutralizer design includes a permanent magnet, any unwanted attitude disturbance due to interaction with the Earth's magnetic field can be compensated with a magnetic dipole that is equal in magnitude and opposite in direction to that of the neutralizer.

The alternative neutralizer design of an early prototype is shown in Fig. 12. A highly iterative approach has been adopted in the development of the neutralizer. The proof-of-concept prototype has a modular design, allowing testing of different configurations. This includes a variation of orifice size and layout to investigate the effects of electron extraction geometry and an increase in neutral density above the nominal  $5 \times 10^{18} \text{ m}^{-3}$  design, for which the orifice spans the full internal chamber diameter. The impact of a range of microwave cavity materials on the performance and degradation through exposure to hot air plasma is assessed, such as the use of Aluminium, Stainless Steel and Molybdenum. Propellant injection schemes are also investigated, namely lateral and rear injection as shown in Fig. 12. For instance, the lateral injection scheme is intended to maximise neutral density in the antenna vicinity where the electric field is maximum, thereby easing ignition. At the end of the neutralizer development, the final prototype version will be integrated and tested as part of the full AETHER system.

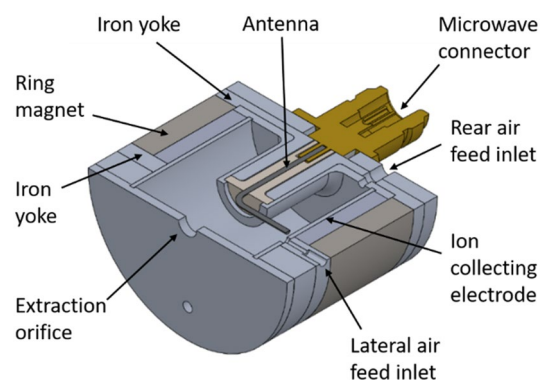
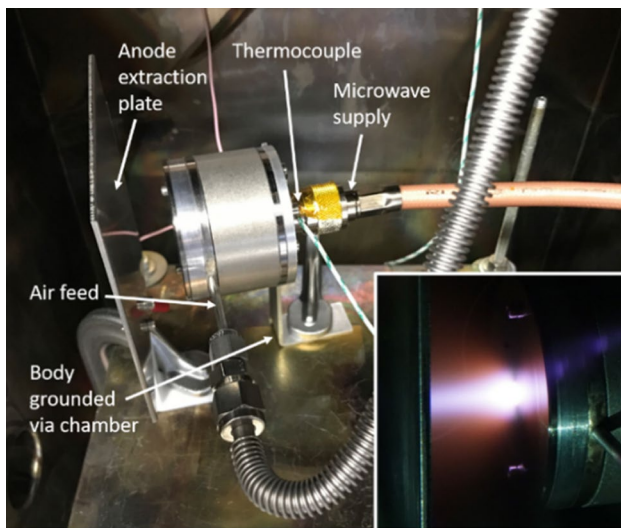


Fig. 12 Cross-section of alternative neutralizer prototype design

The RF neutralizer prototype is tested in stand-alone conditions inside a vacuum chamber, where an anode plate with a positive bias relative to the ion-collecting electrode is used to simulate the thruster plume. This is shown in Fig. 13. For initial tests, the potential difference is established through a positive bias of the anode plate and grounding of the entire neutralizer assembly, however, the internal ion-collecting electrode will be independently biased in more advanced prototype iterations. The air feed tube is brazed through the downstream iron yoke to minimise losses resulting from leaks and a high-temperature microwave cable is used to reduce the influence of temperature effects on the performance. A cylinder of compressed air in the mixture of 52%



**Fig. 13** Alternative neutralizer prototype test setup within vacuum chamber, showing plasma discharge with 0.1 mg/s mass flow rate of 52%  $N_2$  and 48%  $O_2$  air mix at 60 W forward microwave power and 120 V relative bias voltage

$N_2$  and 48%  $O_2$  is used for the tests to approximate the composition in VLEO, although O is necessarily substituted with  $O_2$ . The tests are performed by sequentially varying the air mass flow rate, anode bias voltage and transmitted microwave power (forward minus reflected power monitored by the microwave generator) to record the effect on extracted current, which is measured as the average value displayed on the anode power supply. Successful plasma ignition and current extraction has been demonstrated for several versions of the neutralizer prototype.

## 5.2 Hollow cathode/neutralizer

Due to the criticality associated with the cathode/neutralizer operation with atmospheric propellant, within AETHER activities, we have investigated the behavior of SITAEL's 8-20A LaB6 hollow cathode HC20h with  $N_2$  and  $N_2/O_2$  mixture propellants, see Fig. 14. The typical mono-channel hollow cathode includes an active thermionic electron emitter placed inside a tube, which in the emitter region is often wrapped by a heating element and covered with thermal shield. The whole assembly is enclosed in an electrode, called keeper, used to help the cathode ignition by applying a positive potential with respect to the inner tube. The keeper also protects the internal components from ion bombardment damage.

SITAEL have been developing hollow cathodes of various current levels in the range of 1–100 A. Originally HC20h was designed to operate with Xe propellant. However, during the test campaign it demonstrated the compatibility of its design with the  $N_2$  propellant. With pure nitrogen cathode successfully operated and ignited with similar voltage levels of those with Xe, being able to provide the required current. Pure nitrogen operation resulted in voltage values more than 150% higher than those with Xe for the same molecular

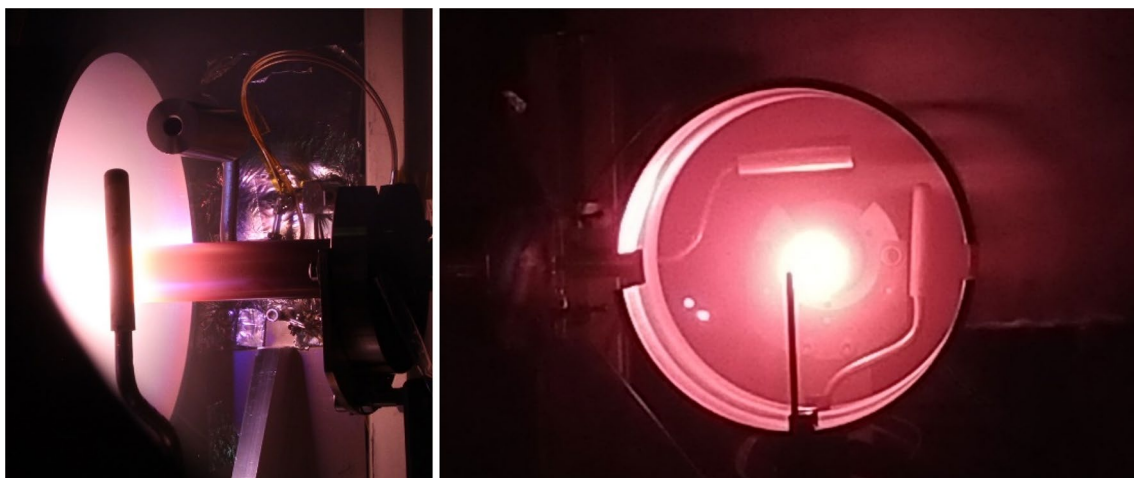


**Fig. 14** HC20h operating on nitrogen (left) and  $Xe/N_2/O_2$  mixture (right)

number density.  $N_2$  operation required higher minimum particle flow rate ( $N_2$ ) at the same current necessary for the cathode stable operation. The Xe reference performance test, held after the operation with  $N_2$ , demonstrated no performance degradation.

The test with the mixture of the  $Xe/N_2/O_2$  was performed after the test with pure  $N_2$  on the same test set-up. The cathode was kept in a keeper triode mode operating on Xe when the atmospheric propellant mixture  $N_2/O_2$  (52%/48%) started being slowly added. When the mass flow rate of the atmospheric propellant reached 11.5% of the total one, numerous sparks were observed in the plume, forcing the test to be terminated.

Cathode reference performance with Xe after the operation with the atmospheric mix propellant demonstrated anode voltage values  $> 200\%$  higher than those before. After an hour of operation with Xe, the anode voltage and keeper ignition voltage were  $> 150\%$  higher than that during the initial Xe characterization. The post-test inspection of the cathode after the atmospheric propellant test has shown a severe erosion and embrittlement of the cathode tube and of some ceramic elements. On the anode, an electrically isolating layer formed, which disappeared after one week of exposure to atmospheric conditions.

## 6 On-ground testing and verification

One of the main challenges in developing a ram-EP system, apart from the technology per se, is the capability of reproducing on-ground a representative environment for actual air-breathing operation. As a matter of fact, this implies the need to provide an extremely rarefied and highly hypersonic flow to the system intake, with number densities on the order of  $1e14$  to  $1e18$   $m^{-3}$  (100 to 250 km altitude

range) and velocities on the order of 8 km/s. Interestingly, data extrapolated from experimental studies on 1 kW-class HETs operating with alternative propellants (containing a high percentage of  $O_2$  and  $N_2$ ) showed that Hall thrusters plume properties are (in terms of averaged velocity and number density of ionized and neutral species) suitable for the on-ground testing of ram-EP systems [36]. In the only concept to date tested in air-breathing mode [12], the VLEO atmospheric flow was simulated by an air-propellant fed Hall thruster (referred to as PFG—Particle Flow Generator) placed in front of the system intake, see Fig. 15.

In this regard, SITAEL's HT5k 5 kW class Hall thruster was selected as a PFG—Particle Flow Generator also for AETHER's activities, see Fig. 16, and has been extensively characterized with atmospheric propellant during the program. The goal of the PFG characterization tests was to better quantify, with respect to past test activities, the level of thruster plume representativeness of VLEO environment. To do this, the diagnostic setup developed in the framework of the project included both invasive and non-invasive diagnostics, together with a set of simulation tools and material samples to be exposed to the thruster plume so to verify materials resistance to atmospheric plasmas. In this regard, test output will allow to quantitatively investigate critical aspects of the end-to-end system setup shows of Fig. 15. A major point which will be addressed and verified as part of the projects is the interaction among the PFG plasma plume and the ram-EP system intake.

### 6.1 Invasive diagnostics

Among the invasive diagnostics to be used, triple Langmuir probes, Faraday cups and Retarding Potential Analyzer (RPA) allowed to measure the PFG plume plasma properties.

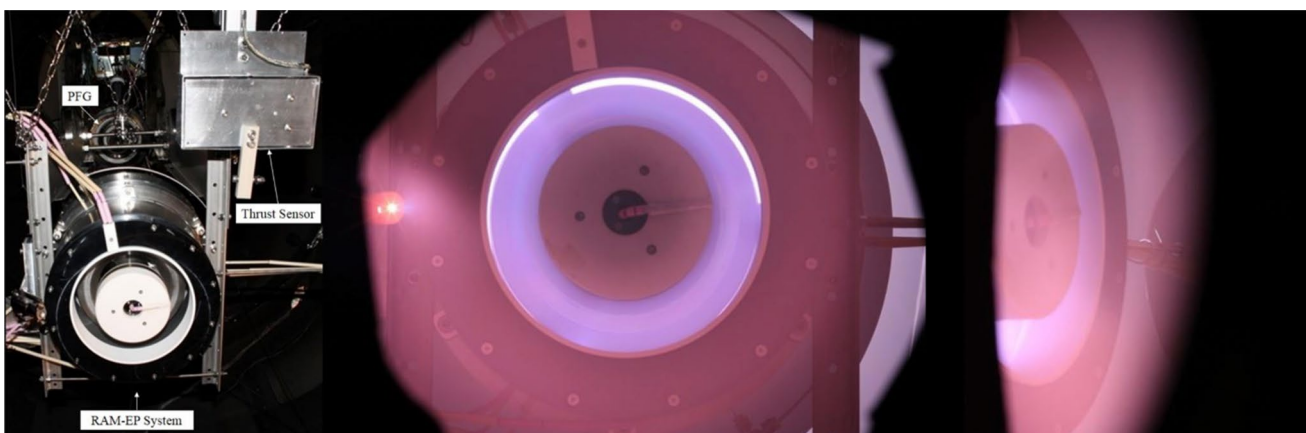


**Fig. 15** Left: Test setup realized for the first demonstration of a thruster operating in air-breathing mode. An atmospheric propellant fed Hall thruster, called PFG and acting as a VLEO flow simulator,

is placed in front of the ram-EP system inlet. Right: Ram-EP system operating with the flow produced by the PFG and gathered by the system intake. Pictures reproduced from [12]



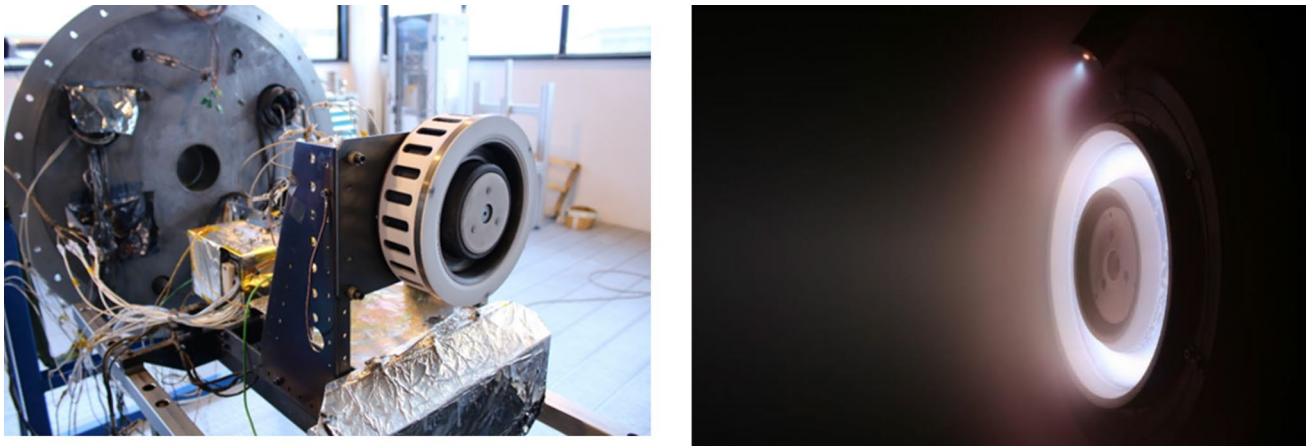


**Fig. 16** Left: HT5k-DM3 installed on its thrust stand. Right: HT5k-DM1 firing with 4.7 mg/s pure 1.27N<sub>2</sub>+O<sub>2</sub> mixture

Triple Langmuir probe is a plasma diagnostic device constituted by three electrodes that allow for the instantaneous measurement of the plasma density, potential, and electron temperature. Triple Langmuir probes do not need a potential sweep to gather information on the plasma parameters and are, thus, particularly suited to investigate plasma regions where the maximum residence time is constrained. The triple Langmuir probe is installed on a mechanical arm, connected to the PFG thrust balance. The dedicated arm supports the probe and allows for its rapid insertion and retraction from the plasma domain. During motion the arm, the probe performs a circular trajectory with a radius of 350 mm. The acquisition is only performed in the final 0.27 rad arc of the probe motion in the near plume and channel region of the thruster.

A movable semi-circular rack of Faraday probes is installed in IV10, the vacuum facility in which the PFG testing will take place. The rack is capable of a complete plume scan at a fixed radial distance from the thruster exit plane, measuring the ion current density distribution in the plume. The analysis of the Faraday probes data allows to assess the plume divergence and thrust vector misalignment.

The RPA probe is integrated in the same movable semi-circular rack hosting the Faraday probes. It is a plasma diagnostic tool which allows to obtain the ion energy distribution in the plasma thruster plume. The working principle of RPA is based on an electrostatic filtering of the plasma particles, allowing only the ions with energy higher than the threshold to reach the probe's collecting electrode. The flux of these ions is measured as a current, which is function of the energy threshold selected by sweeping the probe potential within the energy range of interest. According to its design specification, SITAEL's RPA is capable of measuring ion energies up to 3000 V.

## 6.2 Non-invasive diagnostics

The near-field radiation signature of the PFG plume has been recorded using Optical Emission Spectroscopy (OES) in the Visible and Near InfraRed regions where the electronic transitions occur. Plasma emission is collected by a 25.4 mm diameter collimating lens mounted inside the vacuum chamber at a distance of 300 mm beneath the PFG centerline. The optical collimator is coupled to a 600  $\mu\text{m}$  diameter fiber that brought the signal to a spectrometer system on the in-air side via a dedicated vacuum feedthrough. Spectral emission profiles are measured along spans of 13 equally spaced cross sections perpendicular to the PFG plume axis. The emission magnitudes is calibrated using an integrating sphere light source with a known spectral radiance. Under the assumption of an optically thin axisymmetric plasma, the line-of-sight emission measurements can be Abel-inverted to obtain the local intensity distribution. When the spectral features are not congested, inverted measurements can be used to evaluate the population densities of excited electronic states. The measured densities are then reproduced using a collisional-radiative model to estimate the plasma parameters.

## 6.3 Material assessment

Within all the relevant components required for the AETHER system, materials with different properties and functionalities are required. The materials used in the different components and subsystems includes light weight structural components, ceramics for electrical insulation, magnetic materials, high electrically conductive materials for electrodes, etc. Based on the challenging environmental conditions which these materials are exposed to (atomic oxygen, high temperatures, thermal cycles, as well as plasma exposure), it is necessary to assess the impact of



these conditions on the material performance. Within a literature analysis, first data were collected allowing to identify materials which show a good resistance when exposed to atomic oxygen. This allowed a first identification of suitable material candidates used for electrodes, structural parts, coatings or for insulation. Since in the literature, different plasma conditions or geometric setups were used it is difficult to compare the impact of various multiple environmental conditions acting at the same time (temperature, atomic oxygen, ionized particles) on material characteristics. Therefore, within AETHER, the performance of various materials is analyzed after they are exposed to the conditions in the PFG. In total, more than 20 different material candidates have been selected and were exposed directly to the PFG plume (central position), while in a second configuration, the samples were placed next to the PFG to simulate different plasma and atomic oxygen exposure rates (off-axis position). For all the selected materials, the material removal rate will be determined and the impact of the applied PFG conditions on the material's microstructure will be assessed. Especially if there are reaction products formed will be analyzed by means of Scanning Electron Microscopy (SEM) and X-Ray Diffraction (XRD) analysis. The detailed analysis will allow to confirm which type of materials will survive the harsh environmental conditions in the PFG plume.

#### 6.4 Thermo-chemical plasma modelling

During ground tests, the PFG discharge differs from flight conditions in the thermo-chemical sense, possibly leading to a different gas-surface interaction environment than that expected in orbit. Therefore, it is important to characterize the foreseen experimental plasma. Also, thermo-chemical modelling of the PFG plume can give an insight into the

chemical environment that will be present inside the thruster, thus ensuring understanding of possible issues that may arise over long firings. As part of on-going modelling activities, the chemical evolution of the PFG plume was preliminarily simulated using a time-dependent electronic-specific collisional-radiative model [37–39] accounting for electron-impact chemical processes and spontaneous radiative emission under the assumption of an optically thin plasma. The dynamics of the electronic levels at given densities ( $7e-7 \text{ kg/m}^3$ ) and free-electron temperatures was analyzed based on an a priori analysis of the flow by a simplified and chemically frozen fluid model. An initial concentration of 0.05% was used for the free electrons, which is consistent with the concentration of ions estimated by the baseline model. The free-electron temperature is the driver parameter of the chemical dynamics, and, in the absence of accurate estimates, its value was the subject of a parametric study. Simulations showed that, at the PFG outlet, free-electron temperatures are high enough to justify a flow partially dissociated and significantly ionized. Only ground and metastable energy states of neutral atomic species (N and O) were significantly populated. Charged atomic species dominated steady-state compositions. The concentrations of molecular ions end up being more prominent than those of neutral atomic species.

Figure 17 shows the modeled chemical evolution to steady state of the species and electronic oxygen levels for an electron temperature of 5 eV. The streamline curvilinear abscissa "s" is normalized by the distance between the PFG outlet and the ram-EP intake in the experimental setup,  $L=0.5 \text{ m}$ . This normalization allows the reader to quickly compare the kinetic time scales to the convective time scale of the flow. The mechanism takes about 10 PFG-intake distances  $L$  to reach a steady state

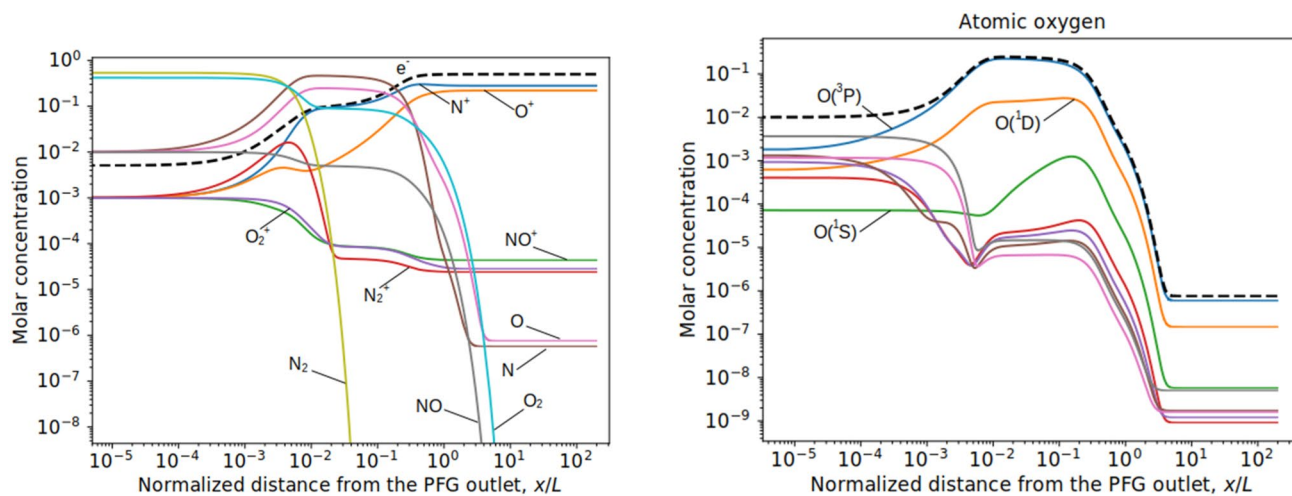


Fig. 17 Chemical evolution to the steady state of the species and electronic oxygen levels for a temperature of 5 eV

## 6.5 AETHER testing approach and development roadmap

Based on the plasma diagnostic and simulation tools presented above, it is apparent how testing activities are at the core of the AETHER programme. As shown in Fig. 18, experimental verifications at both component and system level are scheduled during the project. In more details, testing activities can be divided in four different campaigns.

The first campaign is focused on the verification of both hollow cathode and RF cathode pipe-fed operation with atmospheric and pure  $N_2$  propellant. These activities, performed at the beginning of 2021, have been discussed in Sect. 5. The development of the alternative neutralizer is informed by standalone testing at the University of Surrey. A notable output was the demonstration and characterization of hollow cathode operation with pure  $N_2$  propellant. As such, an  $N_2$ -fed hollow cathode was employed as part of the PFG test setup, allowing to increase significantly the PFG representativeness of VLEO. Indeed, a Xe-fed hollow cathode was needed during past test activities. In AETHER, no Xe will contaminate the VLEO flow reproduced on-ground.

The second campaign is dedicated to the verification of the particle flow generator. In 2021, the PFG, consisting of atmospheric propellant fed HT5k Hall thruster and  $N_2$ -fed HC20 hollow cathode has been characterized in vacuum facility as described in the previous section. The test provided valuable data to validate a model for Hall thruster atmospheric plasma discharge and allowed for a quantitative assessment of VLEO reproducibility on-ground. The PFG test output is fundamental to assess the optimum end-to-end system test setup configuration in terms of PFG operating point and relative intake inlet–PFG distance. Moreover, the material samples included as part of this test setup allowed to better assess atmospheric plasma–material compatibility, allowing to draw verified guidelines for material selection for air-breathing EP devices.

The third campaign concerns the stand-alone testing of the two thruster configurations, the CSAS and CDAS. Stand-alone CSAS testing activities to validate the compliance of the design to the requirements and possibility to operate in the range of predicted performances will be performed upon CSAS components manufacturing, assembly and integration. To perform that test, a Radio Frequency plasma source will be designed, manufactured, and built and together with

the CSAS will constitute practically a Radio Frequency Ion Thruster (RIT). The RIT with the CSAS will be installed in the vacuum test facility and performance characterization on different combinations between mass flows and RF power will be undertaken for both Xe and  $N_2$ – $O_2$  propellants in the thrust range from 6 to 24 mN. It is expected that lower RF power injection would correspond to higher dissociation of the  $N_2$  and  $O_2$  in the discharge for the same thrust level. Stand-alone verification of the thruster assembly in CDAS configuration is scheduled for 2022. The thruster open inlet will be covered by means of a GSE cover, see IV, and the thruster will be characterized in SITAEL's IV10 vacuum facility with propellant fed by the auxiliary propellant injector. The test output will provide thruster performance in terms of thrust, discharge and auxiliary power consumption vs inlet atmospheric propellant mass flowrate and composition and voltage applied to the thruster electrodes. A successful test outcome will increase the confidence in thruster operation in air-breathing mode and allow to preliminarily validate the system performance model.

As a last test campaign, the end-to-end system validation will be performed within end of 2022. The test setup will consist of the PFG operating at its selected operating condition to reproduce VLEO environment and placed in front of the system intake inlet. System operation in air-breathing mode will be verified vs PFG operating point and relative intake inlet–PFG distance. For this test, a reduced-scale intake design will be designed, especially based on the experimental results to be gathered during the previous testing activities. The intake test model will be compatible with the ram-EP thrust balance envelope requirements and will ensure flow properties as representative as possible inside the thruster control volume.

## 7 Conclusions

The possibility to operate a spacecraft in very-low Earth orbits for an extended period may represent a disruptive change in the existing space market. The concept of air-breathing electric propulsion has the ambition to overcome the limitations—in terms of spacecraft mass, cost, and lifetime—imposed by on-board propellant, and to allow the exploitation of VLEO missions. In the framework of the H2020 Air-breathing Electric Thruster (AETHER) project,

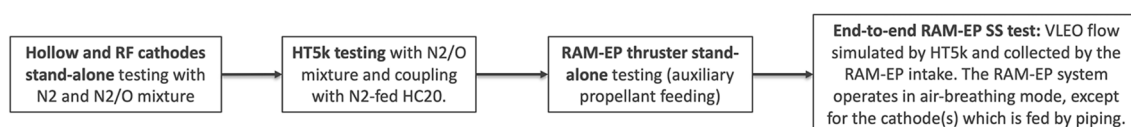


Fig. 18 AETHER testing approach

a consortium of European companies and research institutions (SITAEL, the Von Karman Institute, TransMIT, the University of Surrey, RHP, DEDALOS, and Astos) is aiming at the development of the ram-EP technology. In the present paper, we summarized AETHER activities and we presented the main outcomes of the work performed.

The development of air-breathing electric propulsion relies on an accurate description of the atmospheric flow encountered by the spacecraft along the orbit. This characterization is critical for the calculation of the drag acting on the platform and the optimization of its design, as well as for the generation of thrust from the propulsion subsystem. Thanks to a simple model of thruster operation, it was possible to define a range of altitudes in which full drag compensation seems feasible. As described in the present work, atmospheric properties change significantly with the altitude and the solar activity. Propagations of an air-breathing spacecraft's orbit with time reveal an unavoidable orbital eccentricity at VLEO altitudes (150–250 km) due to the significant effect of the non-sphericity of the Earth's gravity field. The atmospheric properties vary with time, as well as because of the prescribed variation in altitude due to the non-circular orbit. As a result, the thruster system must be robust to changes in the onset flow over both the course of a single orbit or seasonal timescales, without affecting the overall ability to compensate drag.

Based on the requirements derived from the atmospheric flow characterization and the mission analysis, the activities focused on the optimization of the platform aerodynamic design and on the definition of the propulsion subsystem design. In this regard, a fundamental element is the intake that gathers the incoming particles and compresses them before the ionization. State-of-the-art numerical techniques have been adopted to optimize the intake design, highlighting the role of different design solutions in a wide range of design parameters. Constraints related with payload accommodation, platform size and weight were considered in the optimization process.

In parallel with the intake design, two different configurations of an air-breathing thruster have been developed. Both configurations rely on the same ionization stage, which is used for an effective propellant ionization at very low particle densities, thus allowing for an improvement of thruster performance and operation flexibility. The acceleration of ionized particles is then obtained by means of two technological solutions, the first based on crossed magnetic and electric fields, whereas the second is based on charge separation between parallel grids. The two solutions produce an electrostatic acceleration of the ions and guarantee exhaust velocities compatible with the requirement of full drag compensation. A major challenge associated with the adoption of electrostatic acceleration is the operation of the cathode\ neutralizer. While the possibility to operate a traditional

hollow cathode with  $N_2$  and  $O_2/N_2$  mixture was investigated, specific activities have been dedicated to developing an RF neutralizer.

Test activities are an important part of the project, to validate the air-breathing thruster design and to pave the way to the in-orbit demonstration of the technology. The development of an on-ground test bench, which relies on a particle flow generator and advanced diagnostics, is currently on-going. The assessment of material compatibility with the VLEO environment is also proceeding and will drive the design activities. The scheduled test will provide valuable data needed to advance the TRL of air-breathing systems, and successful test outcome is expected to increase the momentum that air-breathing EP gained in recent years. In this regard, several dedicated programmes will then be needed to increase the confidence in the technology and prepare the ground for an IOD mission. Open investigation areas include mission scenario and platform design consolidation, assessment of optimum thrust and power management strategies, identification of ram-EP scaling laws, development of a propulsion system Power Processing Unit and platform intelligence and, from the technological side, development of cathodes capable of operating in air-breathing mode, material characterization and prediction/on-ground verification of thruster lifetime.

**Acknowledgements** The authors would like to express their gratitude to Angela Rossodivita for the coordination of the AETHER activities. Fruitful discussions with Davina Di Cara, Davar Feili, and Vincenzo Pulcino are gratefully acknowledged. This project has received funding from the European Union's *Horizon 2020 Research and Innovation Programme* under grant agreement No. 870436.

## References

1. Crisp, N.H., et al.: The benefits of very low earth orbit for earth observation missions. *Progress Aerosp. Sci.* **117**, 100619 (2020)
2. Fujita, K.: Air intake performance of air breathing ion engines. *J. Japan Soc. Aeronaut. Space Sci.* **52**(610), 514–521 (2004)
3. Fujita, K.: Air intake performance estimation of air-breathing ion engines. *Trans. Jpn. Soc. Mech. Eng.* **70**(700), 3038–3044 (2004)
4. Diamant, K. D.: A 2-Stage Cylindrical Hall Thruster for Air Breathing Electric Propulsion. In: 46th AIAA/ASME/SAE/ASEE Joint Propulsion Conference and Exhibit, Nashville (2010)
5. Hohman, K.: Atmospheric breathing electric thruster for planetary exploration. Final Report, BUSEK Co. Inc. (2012)
6. Schonherr, T., Komurasaki, K., Romano, F., Massuti-Ballester, B., Herdrich G.: Analysis of atmosphere-breathing electric propulsion. *IEEE Trans. Plasma Sci.* **43**, 287–294 (2015)
7. Barral, S. Cifali, G. et al.: Conceptual design of an air-breathing electric propulsion system. In: 34th International Electric Propulsion Conference, Hyogo-Kobe, Japan (2015)
8. Erofeev, A.I., et al.: Air-breathing ramjet electric propulsion for controlling low-orbit spacecraft motion to compensate for aerodynamic drag. *Sol. Syst. Res.* **51**, 639–645 (2017)
9. Romano, F., Massuti-Ballester, B., et al.: System analysis and test-bed for an atmosphere-breathing electric propulsion system

- using an inductive plasma thruster. *Acta Astronaut.* **147**, 114–126 (2018)
10. Marchioni, F.: Design and Performance Measurements of a Long Channel Hall Thruster for Air-Breathing Electric Propulsion. Master's Thesis, Politecnico di Torino, (2020)
  11. Zheng, P., Wu, J., Zhang, Y., Wu, B.: A Comprehensive review of atmosphere-breathing electric propulsion systems. *Int. J. Aerosp. Eng.* **2020**, 8811847 (2020)
  12. Andreussi, T., Ferrato, E., Piragino, A., Cifali, G., Rossodivita, A., Andrenucci, M., Longo, J., Walpot, L.: Development and experimental validation of a Hall effect thruster RAM-EP Concept. In: 35th International Electric Propulsion Conference, Atlanta, Georgia, 8–12 October 2017, IEPC-2017–377 (2017)
  13. Andreussi, T., Ferrato, E., Giannetti, V., Piragino, A., Cifali, G., Andrenucci, M., Paisonni, C. A.: Development status and way forward of SITAEL's air-breathing electric propulsion engine. In: AIAA Propulsion and Energy Forum and Exposition 2019, Indianapolis, Indiana 19–22 August (2019)
  14. Ferrato, E., Giannetti, V., Piragino, A., Andrenucci, M., Andreussi, T., Paisonni, C. A.: Development roadmap of SITAEL's RAM-EP system. In: 36th International Electric Propulsion Conference, Vienna, Austria, 15–20 September 2019, IEPC 2019–886 (2019)
  15. Tisaev, M., Ferrato, E., Giannetti, V., Paisonni, C., Baresi, N., Lucca Fabris, A., Andreussi, T.: Air-breathing electric propulsion: flight envelope identification and development of control for long-term orbital stability. *Acta Astronaut.* **191**(October 2021), 374–393 (2022)
  16. Ferrato, E., Giannetti, V., Tisaev, M., Lucca Fabris, A., Califano, F., Andreussi, T.: Rarefied flow simulation of conical intake and plasma thruster for very low earth orbit spaceflight. *Front. Phys.* **10**(March), 1–17 (2022)
  17. Steiger, C., Romanazzo, M., Paolo Emanuelli, P., Floberghagen, R., Fehring, M.: The Deorbiting of ESA's Gravity Mission GOCE—Spacecraft Operations in Extreme Drag Conditions. In: AIAA 2014–1934 Session: OCMSA—End of Life Operations. <https://doi.org/10.2514/6.2014-1934>
  18. Berenguer, Ch., Katsonis, K.: Evaluation of earth atmosphere remnants used as propellant in electric thruster technology. In: 7th Space Propulsion 2020+1 Conference, SP2020\_018, Estoril, Portugal, (2021)
  19. Katsonis, K., Berenguer, Ch., Walpot, L., Gonzalez Del Amo, J.: A Detailed Global Model of Hydrogen / Helium in Support of Neptune Study. In: 7th Space Propulsion 2020+1 Conference, SP2020\_384, Estoril, Portugal (2021)
  20. Katsonis, K., Berenguer, Ch., Cesaretti, G.: ISRU technology propulsion for missions in the solar system. In: 1st Aerospace Europe Conference 2020, AEC2020\_523, Bordeaux, France, 25 to 28 February 2020
  21. Katsonis, K., Berenguer, Ch.: Report DEDA-AETH-PD-0204 Is.1.1. Review of the Atmospheric Propellants. Thessaloniki, Greece, September 20, 2020.
  22. Picone, J.M., Hedin, A.E., Drob, D.P., Aikin, A.C.: NRL-MSISE-00 empirical model of the atmosphere: statistical comparisons and scientific issues. *J. Geophys. Res.* **107**, 1468 (2002)
  23. Hedin, A.E.: Extension of the MSIS thermospheric model into the middle and lower atmosphere. *J. Geophys. Res.* **96**, 1159 (1991)
  24. Di Cara, D., Gonzalez del Amo, J., Santovincenzo, A., Carnicero Dominguez, B., Arcioni, M., Caldwell, A., Roma, I.: RAM electric propulsion for low earth orbit operation: an ESA study In: 30th IEPC Conference, IEPC-2007–162, Florence, Italy, September 2007.
  25. Lev, D., Myers, R.M., Lemmer, K.M., Kolbeck, J., Koizumi, H., Polzin, K.: The technological and commercial expansion of electric propulsion. *Acta Astronaut.* **159**, 213–227 (2019)
  26. Drinkwater, M.R., Floberghagen, R., Haagmans, R., Muzi, D., Popescu, A.: ESA's First Earth Explorer Core Mission. In: Beutler, G., Drinkwater, M.R., Rummel, R., Von Steiger, R. (eds.) *Earth Gravity Field from Space | From Sensors to Earth Sciences*. Space Sciences Series of ISSI, vol. 17. Springer, Dordrecht (2003)
  27. Schaaf, S.A., Chambre, P.L.: *Flow of Rarefied Gases*. Princeton University Press, Princeton (1961)
  28. Andreussi, T. et al.: AETHER Air Breathing Electric THruster: towards very low earth orbit missions. In Proceedings of the 72nd International Astronautical Congress, Dubai, United Arab Emirates, October 25–29, IAC-21,C4.5,x66453
  29. Curtis, H.: *Orbital mechanics for engineering students*, p. 177. Elsevier, Butterworth-Heinemann (2013). <https://doi.org/10.1016/C2011-0-69685-1>
  30. Verstraete, T.: *Multidisciplinary Turbomachinery Component Optimization Considering Performance, Stress and Internal Heat Transfer*. Ph.D. thesis, University of Ghent / von Karman Institute for Fluid Dynamics (2008)
  31. Parodi, P.: *Analysis and simulation of an intake for air-breathing electric propulsion systems*. M.S. thesis, University of Pisa (2019)
  32. Verstraete, T., Mueller, L., Aissa, M.H.: *Multidisciplinary optimization of turbomachinery components using differential evolution*. VKI Lecture Series, von Karman Institute for Fluid Dynamics (2018)
  33. Geuzaine, C.G., Remacle, J.F.: *Gmsh: a three-dimensional finite element mesh generator with built-in pre- and post-processing facilities*. *Int. J. Numer. Methods Eng.* **79**(11), 1309–1331 (2009)
  34. Funaki, I., Kuninaka, H.: *Overdense plasma production in a low-power microwave discharge electron source*. *Jpn. J. Appl. Phys.* **40**(1,4A), 2495–2500 (2001)
  35. Chen, F.F.: *Introduction to Plasma Physics and Controlled Fusion*. Springer, New York (1984)
  36. Cifali, G., Misuri, T., Rossetti, P., Andrenucci, M., Valentian, D., Feili, D., Lotz, B.: *Experimental Characterization of HET and RIT with Atmospheric Propellants*. IEPC-2011–224 (2011)
  37. Bultel, A., et al.: *Collisional-radiative model in air for earth re-entry problems*. *Phys. Plasmas* **13**(4), 11 (2006)
  38. Huo, W.M., Panesi, M., Magin, T.E.: *Ionization Phenomena behind Shock Waves*. Encyclopedia on Shock Waves. Springer, New York (2011)
  39. Panesi, M., et al.: *Fire II flight experiment analysis by means of a collisional-radiative model*. *J. Thermophys. Heat Transfer* **23**(2), 236–248 (2009)

**Publisher's Note** Springer Nature remains neutral with regard to jurisdictional claims in published maps and institutional affiliations.